



DEGREE PROJECT IN ELECTRICAL ENGINEERING,
SECOND CYCLE, 30 CREDITS
STOCKHOLM, SWEDEN 2019

Antenna Design for Angle of Arrival Measurement in Access Control Applications

THEODOROS PROKIC

Antenna Design for Angle of Arrival Measurement in Access Control Applications

THEODOROS PROKIC

Master in Wireless Systems

Date: March 23, 2019

Supervisor: Mahsa Ebrahimpouri Hamlkar

Examiner: Oscar Quevedo Teruel

Swedish title: Antenn konstruktion för Angle of Arrival mätningar i åtkomstkontroll lösningar.

School of Electrical Engineering and Computer Science

Abstract

The Bluetooth direction finding working group proposed functionalities to the Bluetooth core that can realize Angle of Arrival estimations using interferometry. The technology can be employed to develop new access control applications. Following previous findings in Englund (2018), the purpose of this project is to investigate the feasibility of such systems when antennas are being used. The goal is to design a matchbox size antenna array which can be used by the system to distinguish between two sides in an inside-outside scenario. A number of antennas were designed, simulated and tested on a prototype. While the simulations results were consistent with the theory, the prototype measurements were not. However, it is shown that it is possible to estimate between inside and outside.

Keywords: Patch Antenna, Angle of Arrival, Bluetooth, Keyless Access Control

Sammanfattning

Bluetooth direction finding working group har lagt fram ett förslag om att lägga till Angle of Arrival estimerings funktionalitet baserat på en interferometri metod i Bluetooth kärnan. Tekniken kan användas för att utveckla nya åtkomstkontrolls lösningar. Detta projekt en påbyggnad av arbetet utfört av Englund (2018), syftet är att utvärdera möjligheten av en sådan åtkomstkontrolls lösning där antenner används. Målet är att designa en tändsticksask stor antenn array som kan användas av ett systemet för att särskilja mellan två sidor i ett insida-utsida scenario. Ett antal antenner konstruerades, simulerades och prototyper byggdes samt testades. Medan simuleringsresultaten var förenliga med teorin, så påvisade prototyperna inte samma beteende då resultatet skiljde sig från teorin. Projektet konstaterar dock att det är möjligt att skilja mellan insida och utsida.

Acknowledgements

First of all, I would like to express my gratitude to Assa Abloy Shared Technologies and in particular to Fredrik Einberg, Mattias Haeger and Mats Cederblad. This project could not have finished without their invaluable guidance and support. It was a fantastic opportunity to conduct my project in the research and development department among engineers of high caliber.

I am very thankful to my supervisor Mahsa Ebrahimpouri Hamlkar and my examiner Oscar Quevedo Teruel for their valuable feedback. They were always happy to provide answers and I have learned a lot from them.

Special thanks to my partner in crime Martin Englund for the interesting discussions during lunch time.

Finally, I would like to thank to my father, my mother and my sister who no matter what, have supported me through everything. Even if they are miles away it always felt as if they stood by my side.

Contents

1	Introduction	1
1.1	Background	1
1.2	Previous work and research gaps	2
1.3	Problem Definition	3
1.4	Contribution	3
1.5	Objectives	4
1.6	Methodology	4
1.7	Outline	5
2	Background Knowledge	6
2.1	Introduction to Antennas	6
2.2	Fundamental Antenna Parameters	7
2.2.1	Frequency	8
2.2.2	Reciprocity	8
2.2.3	Radiation Pattern	8
2.2.4	Directivity	9
2.2.5	Efficiency	10
2.2.6	Gain	10
2.2.7	Field Regions	11
2.2.8	Bandwidth	12
2.2.9	Input impedance	13
2.2.10	Coupling	13
2.2.11	Antenna Isolation	14
2.2.12	Polarization	14
2.3	Patch Antennas	15
2.3.1	Working Principle	15
2.4	Substrate	17
2.5	Path Loss Model	18
2.6	Angle of Arrival	20

2.7	Bluetooth Low Energy Standards	22
2.8	Evaluation Method	23
2.8.1	IQ Sampling	23
2.8.2	Time to Phase	23
2.8.3	Phase Difference Calculation	24
3	Challenges for AoA Antenna Solution	26
3.1	Orientation and polarization	26
3.2	AoA Antenna Switching Board Matching	27
3.3	Coupling	28
3.4	Reflections	28
3.5	Distance	29
3.6	Interference	29
3.7	Size	29
3.8	Phase Center	29
4	Antenna Design	30
4.1	Square Ring Meandered Antenna	31
4.1.1	Simulation	31
4.1.2	Measurements	33
4.2	Normal Patch Antenna	35
4.2.1	Simulation	35
4.2.2	Measurements	36
4.3	Circularly Polarized Patch Antenna	38
4.3.1	Simulations	38
4.3.2	Measurements	41
4.3.3	Improvement	44
4.4	Standard Patch Antenna	44
5	Evaluation Setup	46
5.1	CST Microwave Studio	46
5.2	Test setup	47
5.3	Texas Instruments Evaluation Board	50
5.4	Texas Instruments Antenna Credential	51
5.5	Radio Frequency Anechoic Chamber	54
5.6	Line of Sight	55
5.7	Wooden Door	55
5.8	Metal Door	55

6	Results and Discussion	56
6.1	First Iteration	59
6.1.1	Square Ring Antenna	59
6.1.2	NPA	63
6.1.3	Circularly Polarized Patch Antenna	67
6.1.4	Summary	72
6.2	Second Iteration	73
6.2.1	SPA	73
6.2.2	Credential Orientation	89
7	Conclusion	93
7.1	Future studies	94
	References	95

List of Figures

1.1	The problem.	4
2.1	Transmission-line Thevenin equivalent of antenna in transmitting mode.	7
2.2	The radiation pattern of a dipole antenna operating at 2.4 GHZ.	9
2.3	The directivity of a dipole antenna operating at 2.4 GHZ.	10
2.4	The gain of a dipole antenna operating at 2.4 GHZ.	11
2.5	Field regions surrounding an antenna.	12
2.6	Input impedance of a dipole operating at 2.4 GHz.	13
2.7	Side view of a patch antenna.	15
2.8	Side view of a patch antenna with electric fields in the substrate.	16
2.9	Receiving antenna gain requirement	20
2.10	Two antenna elements and an incoming planar wave.	21
2.11	Two antenna elements and two incoming planar waves.	22
2.12	IQ sampling scheme.	23
2.13	Phase difference calculation using four-quadrant inverse tangent.	25
3.1	Switching board during sampling.	27
3.2	Switching board during termination.	28
4.1	Dimensions of the Square Ring Meandered Antenna.	32
4.2	S_{11} parameters of the Square Ring Meandered Antenna.	32
4.3	Gain parameters of the Square Ring Meandered Antenna.	33
4.4	Axial ratio of the Square Ring Meandered Antenna.	33
4.5	Manufactured Square Ring Meandered Antenna.	34
4.6	S_{11} parameters of the Manufactured Square Ring Meandered Antenna.	34

4.7	Dimensions of the Normal Patch Antenna.	35
4.8	The S_{11} parameters of the Normal Patch Antenna.	36
4.9	Gain of the Normal Patch Antenna.	36
4.10	Manufactured Normal Patch Antenna.	37
4.11	Measured S_{11} parameters of the Normal Patch Antenna.	37
4.12	The dimensions of the two circularly polarized patch antennas.	39
4.13	The S_{11} parameters of the two circularly polarized patch antennas.	40
4.14	The gain of the two circularly polarized patch antennas.	41
4.15	The manufactured circularly polarized patch antennas.	42
4.16	The S_{11} parameters of the two circularly polarized patch antennas.	43
4.17	The dimensions of the SPA	44
4.18	The S-parameters of the SPA	45
4.19	The gain of the SPA	45
5.1	Simulation setup.	46
5.2	Test setup.	47
5.3	One test setup from two different angles.	48
5.4	A simplified model of Figure 5.3.	49
5.5	The CC2640R2 Development Kit.	51
5.6	Texas Instruments 2.4-GHz Inverted F Antenna.	51
5.7	The slot antenna and the dipole antenna.	53
5.8	Measured reflection at the feed point of the antenna.	54
6.1	Angle of Arrival theoretical results.	56
6.2	Angle of Arrival Estimation using delaylines.	57
6.3	Reference line and angle measurement in comparison to the antenna placement	58
6.4	The two square ring meandered antennas on test site.	59
6.5	Simulated phase differences between the two square ring meandered antennas.	60
6.6	Calculated phase differences between the two square ring meandered antennas.	61
6.7	Calculated Angle of Arrival between the two square ring meandered antennas.	62
6.8	Angle of Arrival Estimation using the square ring meandered antennas.	63
6.9	Test setup of the normal patch antennas.	64

6.10	Simulated phase differences between the two normal patch antennas.	64
6.11	Calculated phase differences between the two normal patch antennas.	65
6.12	Calculated Angle of Arrival between the two normal patch antennas.	66
6.13	Angle of Arrival Estimation using the normal patch antennas.	67
6.14	Angle of Arrival Estimation using the circularly polarized patch antennas.	68
6.15	Simulated phase differences between the two circularly polarized patch antennas.	69
6.16	Calculated phase differences between the two circularly polarized patch antennas.	70
6.17	Calculated Angle of Arrival between the two circularly polarized antennas.	71
6.18	Angle of Arrival Estimation using the circularly polarized patch antennas.	72
6.19	Test setup of SPA antennas.	74
6.20	Closeup of test setup of the SPA antennas.	74
6.21	Simulated phase differences between the two standard patch antennas.	75
6.22	Calculated phase differences between the two standard patch antennas.	76
6.23	Angle of Arrival Estimation using the circularly polarized patch antennas.	77
6.24	Angle of arrival estimation using the BSA antennas with arbitrary compensation.	78
6.25	Angle of Arrival Estimation of BSA antennas.	79
6.26	Angle of Arrival Estimation without IQ compensation.	80
6.27	Antenna setup offset at 30°.	81
6.28	Simulated phase differences between the two standard patch antennas (30°).	82
6.29	Calculated phase differences between the two standard patch antennas (30°).	83
6.30	Calculated Angle of Arrival between the standard patch antennas (30°.	84
6.31	Angle of Arrival Estimation using the standard patch antennas (30°).	85

6.32	Angle of Arrival Estimation using the standard patch antennas (30°) after filtering.	86
6.33	The three antenna system.	87
6.34	The resulting angles from the three different antennas.	88
6.35	Two different orientations of the credential.	89
6.36	The resulting angles from the two different orientations of the credential.	90
6.37	The three different distances.	91
6.38	The resulting angles from the difference in the distance between the antenna elements.	92
7.1	A potential use of AoA in access control applications.	94

List of Tables

2.1	Bandwidth of 4 different antennas	12
2.2	Impact of different substrates.	18
2.3	Advertising channel center frequencies	22
3.1	Impact of different polarization between transmitter and receiver	27
5.1	IFA Dimensions	52
5.2	Gain in different orientations for the TI IFA.	55

Chapter 1

Introduction

Traditionally, electronic physical access control is based on presenting RFID cards to a reader or digital door lock. With the advent of Bluetooth Low Energy, using the mobile phone as an access credential is getting common. ASSA ABLOY has several so called Mobile access solutions in place for both commercial and residential use. Use of Bluetooth enables so called keyless entry where the mobile credential is left in the pocket and the door unlocks when you approach it. I.e. the concept that is commonly used in new cars. Challenges with all keyless entry solutions is that accurate positioning of the mobile is required. Today, positioning is typically based on signal strength (RSSI) which has its limitations. However, new more accurate RF positioning technologies are emerging. Especially promising are ones based on Angle of Arrival (AoA). The purpose with this master thesis is to evaluate state of the art AoA technology for use in physical access control.

1.1 Background

Today almost everyone owns a smartphone. Statistics shows that the number of smartphone ownership will increase to 2.87 billion by 2020 [1]. In addition the projected size of the global market for RFID tags will be 24.5 billion dollars [2]. The market is growing and the technology is only improving making electronics smaller and more reliable [3].

The benefits of a potential commercial product are enormous. In a keyless entry environment people would not have to use a key to enter

doors. The keys that we are using today could be totally obsolete with this technology. A mobile phone could potentially be the key of the future.

1.2 Previous work and research gaps

There have been a lot of studies in the angle of arrival or direction of arrival technology. They can be divided into conventional methods and unconventional methods [4]. The author gives an overview of the main AoA algorithms. Most of the research promotes signal processing and beamforming. In addition a great amount of studies are not tested in a real life scenario [5]. Most of the studies are researched through simulations and models and while they provide a good insight in the problem, measurements in a real life scenario are needed to approve the studies. There are estimators that when simulated, provide good AoA results such as the MUSIC subspace method [6]. In this paper the author concludes that there were no assumption made about array geometry. A real life scenario was tested in [7] where a multipath AoA localization system was proposed and tested. The authors used a room to test two different algorithms. The frequencies they worked with were 2.4 GHz and 5.2 GHz which fall into the Wi-Fi standard[8]. This is quite important because the study shows that there might be a product implementation.

Most of the studies in literature are concerned with algorithm optimization. In [9] the authors present an AoA estimation using MUSIC algorithm in a real life scenario. In addition they present the antennas used for the measurements. The authors conclude that there is a partial source sensitivity to the AoA estimation. In [10] the authors develop a 2D AoA estimation with antenna arrays. The authors developed a design which takes into consideration the SCF change rates. Similarly, in [11] the authors show the problems that the antenna design can create and algorithms to compensate.

An interesting approach is the [12] study. The authors deployed their own algorithm for estimating the AoA with high accuracy. They used their own antenna design which could potential have product implementations. They present their idea behind the specific choice of antennas and why the design matters. The design is relative to the wavelength of a standardized Wi-Fi frequency. They conclude the

need of additional studies in polarization diversity to solve the 3D direction of arrival. In addition, they argue that by not considering the polarization of the antennas in question, the system could give unreliable AoA angles.

There is very limited literature for specific antenna designs for an AoA solution and the reasoning behind the antenna choice design [13]. In this particular study the authors test two different antenna designs for an AoA estimation algorithm. There are currently no specific guidelines for an antenna solution which utilizes conventional methods for AoA estimation. Most of the studies that have a real life tests are relatively new studies. Therefore the research gap lies on the guidelines of the antenna design for conventional AoA localization solutions.

1.3 Problem Definition

The main purpose of this project is to build and present a solid understanding of antenna requirements for an AoA solution. Depending on those requirements a layout for an antenna solution must be found. Theoretical investigations and simulations need to be conducted in order to find the appropriate design for this project. Firstly evaluating how the antenna elements type, number and arrangement impacts the accuracy of the system. Secondly, the mutual coupling and interference from other sources between the antenna elements impact the system. In the end the surface at which the antennas are placed and potential reflections must be investigated.

1.4 Contribution

The contribution of this thesis is to provide information about the challenges the antenna design faces when an AoA solution is desirable. There are studies that point to the problems engineers are faced when they design the antenna array but there is no consistent set of rules that must be taken into consideration before the design process.

Both companies and individuals will benefit from a set of rules in designing antennas for AoA. Apart from individuals, academic staff could potentially expand the research.

1.5 Objectives

The main objective of this project is to build and present solid understanding of antenna requirements for an AoA solution. The goal of this project is to design and manufacture an antenna operating at 2.4 GHz according to the requirements for an AoA solution. In addition, the size of smallest possible antenna solution providing good accuracy must be investigated. The target size is a match box and more specifically, 5 x 2 x 7 cm. Finally, the impact the environment has on the antenna's accuracy will be investigated.

The accuracy of this project is defined so that the system can recognize if the credential is either on the inside or outside of a potential line that divides the space as seen in Figure 1.1. The red part shows the angles that the credential is on the inside, the yellow part shows uncertainty and the green part show that the credential is on the outside. The inside part covers 180° while the yellow and green parts cover 60° and 120° respectively.



Figure 1.1: The problem.

1.6 Methodology

The methodology this thesis follows can be divided in five distinct parts. The first part involves the **Research**. In this part research will be done on antenna theory and AoA. Books, journals and publication can provide insight into the theory and technology that is available today.

The second part involves the **Antenna Design**. In this part emphasis will be put into the parameters of each antenna element individually and how the elements interact with each other. Simulations will provide some insight on how do the elements interact with the environment surrounding them. After that **Antenna Concept Solution** must be determined. The AoA technology determines the direction of an RF signal by using data received from an array of antenna elements. The arrangement and number of the elements must be taken into consideration so that they can be enclosed in a tight space. During this phase, an arrangement of the antenna elements that can at least partially satisfy all the requirements must be found. Following the **Antenna Concept Solution** is the **Prototype** part. In this part a prototype based on the design provided by the simulations were made. The next part is the **Prototype Evaluation**. Here, evaluation of the prototype with real analyzers will take place. The parameters of the antenna array will be measured and provide a better insight. In addition the AoA tests will be conducted in this part. In the next part **Refine Prototype and Results** a second iteration will be made based on the evaluation from the previous part. In other words, the prototype will be corrected and refined to suit the project's requirements. If time allows, miniaturization techniques will take place to make the prototype as small as possible. Additionally, the rest of the parameters will be refined as well. After the refinement, the final prototype will be finished. Finally the last part is the **Report Writing**. By the time the final prototype is close to finish, focus will be directed to the final report.

1.7 Outline

The thesis is structured in the following way. Chapter 2 provides the terminology and technology, including Angle of Arrival and basic knowledge from antenna theory. Chapter 3 the evaluation setup is described. All the simulation and technical tools involved in the thesis are represented. Chapter 4 provides information about the antennas used as a receiver to the evaluation setup. The choice, design parameters and results are presented in this part. Chapter 5 presents the prototype tests. Chapter 6 summarizes the thesis, gives recommendations for future studies and concludes the thesis.

Chapter 2

Background Knowledge

In this chapter, the background knowledge for the general reader will be given. These are the most fundamental parameters that are essential to understand the project. The fundamental antenna parameters, the path loss model, patch antennas, angle of arrival and the Bluetooth low energy standards will be discussed.

2.1 Introduction to Antennas

The IEEE Standard Definitions of Terms for Antennas defines the antenna as “a means for radiating or receiving radio waves” [14]. Specifically an antenna is the device in-between free space and a guiding device. The guiding device, otherwise known as a transmission line is used to transport the electromagnetic energy from a transmitting source to the antenna or in reverse from an antenna to a receiver [4].

Balanis [4] states that an antenna system can be viewed as a transmission line Thevenin equivalent as shown in figure 2.1.

In figure 2.1 the source is considered ideal. The transmission line is represented by a characteristic impedance of Z_c and the antenna is represented by a load Z_A . R_L represents the dielectric and conduction losses while R_r represents the radiation resistance of the antenna. The reactance X_A represents the imaginary part of the impedance and is associated with radiation by the antenna [4]. The equation for the antenna element and the transmission line can be seen in Equation 2.1.

$$Z_A = (R_L + R_r) + jX_A \quad (2.1)$$

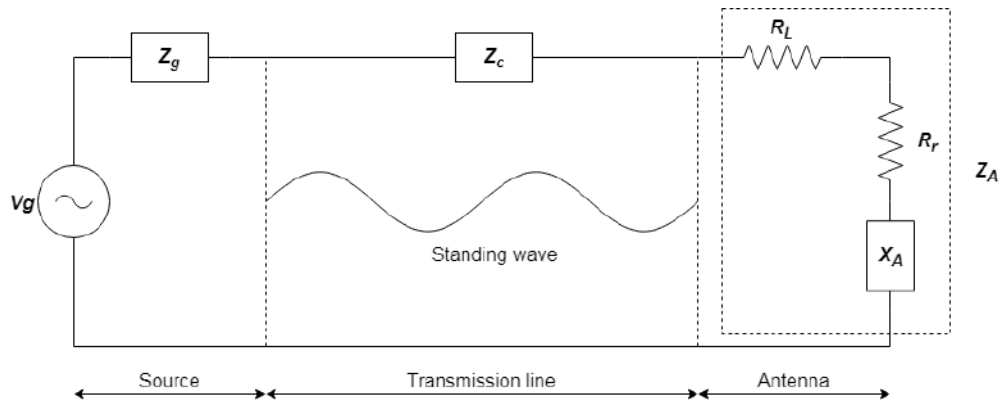


Figure 2.1: Transmission-line Thevenin equivalent of antenna in transmitting mode.

In an ideal world a source transfers power directly to the radiation resistance R_r without loss of power. However, the transmission line and the antenna inherently add conductive and dielectric losses. This is due to the lossy nature of the materials used. Apart from those losses, the system is susceptible to mismatch losses because of the reflections at the border between the transmission line and the antenna. Maximum power delivered to the antenna is achieved when the mismatch losses are zero.

The reflected waves from the border between the transmission line and the antenna are called standing waves. Standing waves exist along the transmission line which can be represent as concentrated pockets of energy.

Therefore the losses that an antenna system has can be divided in transmission line, antenna and standing waves losses. In order to minimize the losses as much as possible, the loss resistance of the antenna R_L must be reduced and the impedance of the antenna must be matched to the characteristic impedance of the transmission-line.

2.2 Fundamental Antenna Parameters

In this section the fundamental antenna parameters for describing an antenna will be briefly explained and discussed.

2.2.1 Frequency

Antennas are working by transmitting and receiving electromagnetic waves. Electromagnetic waves propagate at the speed of light which is $299792458m/s$. A charged particle creates an electric field and it creates ripples or oscillations in its electric field. This also produces a magnetic field [15]. This means that an electric field that oscillates as a function of time will produce a magnetic field and a magnetic field that changes as a function of time will produce an electric field. The two waves create an electromagnetic wave which propagates in the direction perpendicular to plane that the electric and magnetic wave are oscillating. The electromagnetic wave is periodic. It repeats itself every T seconds or λ meters. Equations 2.2 and 2.3 describe this:

$$f = \frac{1}{T} \quad (2.2)$$

$$c = f\lambda \quad (2.3)$$

In other words the frequency describes how fast the electromagnetic wave is oscillating.

2.2.2 Reciprocity

Reciprocity is the characteristic that antennas in transmit and receive modes has the same properties. However reciprocity applies to antennas operating in a linear environment. In other words when designing an antenna system one can investigate the transmit mode of the antenna system [16].

Nevertheless there are circumstances where reciprocity does not apply. Antennas that are made out of magnetic materials that exhibit hysteresis are not linear materials [17].

2.2.3 Radiation Pattern

The radiation pattern is defined as "a mathematical function or a graphical representation of the radiation properties of the antenna as a function of space coordinates. In most cases, the radiation pattern is determined in the far-field region and is represented as a function of the directional coordinates" [14]. It describes the variation of the radiation power in different directions. It is measured in the far-field region of the antenna. Isotropic antennas are antennas which radiate

in every direction with the same power. Isotropic antennas do not exist in reality. The radiation pattern can distinguish antennas between omnidirectional and directional. Omnidirectional means that the radiation pattern is isotropic for one plane [4].

An omnidirectional radiation pattern can be seen in Figure 2.2 describing a dipole antenna operating at 2.4 GHz.

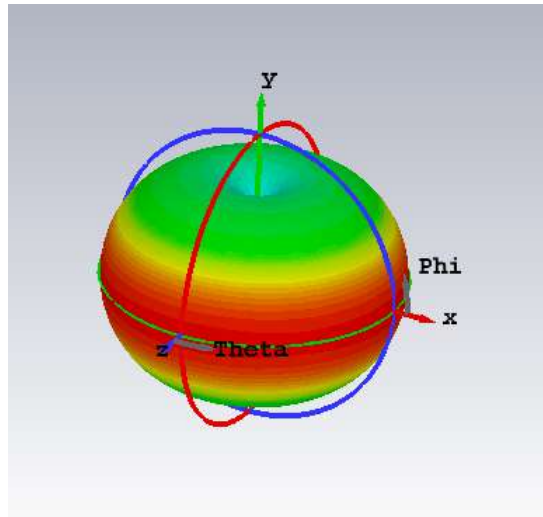


Figure 2.2: The radiation pattern of a dipole antenna operating at 2.4 GHz.

2.2.4 Directivity

Directivity is defined as "the ratio of the radiation intensity in a given direction from the antenna to the radiation intensity averaged over the direction. The average radiation intensity is equal of the total power radiated but the antenna divided by 4π " [18]. An antenna that radiates equally in all directions has a directivity of one[17].

The directivity pattern can be seen in Figure 2.3 describing a dipole antenna operating at 2.4 GHz.

Electrically small antennas that have a quarter of a wavelength to a half of a wavelength length typically minimize directivity. Such antennas are half-wavelength dipoles or quarter-wavelength monopoles.

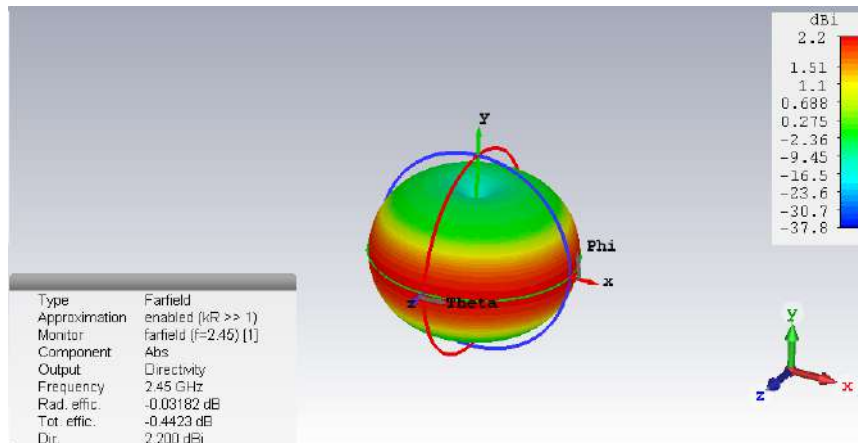


Figure 2.3: The directivity of a dipole antenna operating at 2.4 GHz.

2.2.5 Efficiency

Efficiency is defined as “the ratio between the radiated power of the antenna and the power delivered to the antenna” [17]. An antenna with a high efficiency would radiate most of the power delivered to it, whereas an antenna with a low efficiency would absorb or/and reflect most of the power delivered to it. Equation 2.4 defines efficiency.

$$\varepsilon_R = \frac{P_{\text{radiated}}}{P_{\text{input}}} \quad (2.4)$$

The losses that contribute to antenna efficiency can be attributed to three kind of losses, that is conduction, dielectric and impedance mismatch losses. Efficiency is one of the most important antenna parameters. For example dish and shotgun antennas can have an efficiency which can be very close to 100% when no lossy materials surround them. On the other hand antennas that are use in consumer products such as a mobile phone and Wi-Fi antennas have efficiencies that mostly range between 20% and 70%.

2.2.6 Gain

The gain is defined as “the ratio of the intensity, in a given direction, to the radiation intensity that would be obtained if the power accepted by the antenna were radiated isotropically. The radiation intensity corresponding to the isotropically radiated power is equal to the power accepted by the antenna divide by 4π ” [19]. For example an antenna

having a gain of $3dB$ means that the power received in the far field would be twice as much than the power that would be received by a lossless isotropic antenna when power antennas were fed with the same power.

The gain describing a dipole antenna operating at 2.4 GHz. can be seen in Figure 2.4.

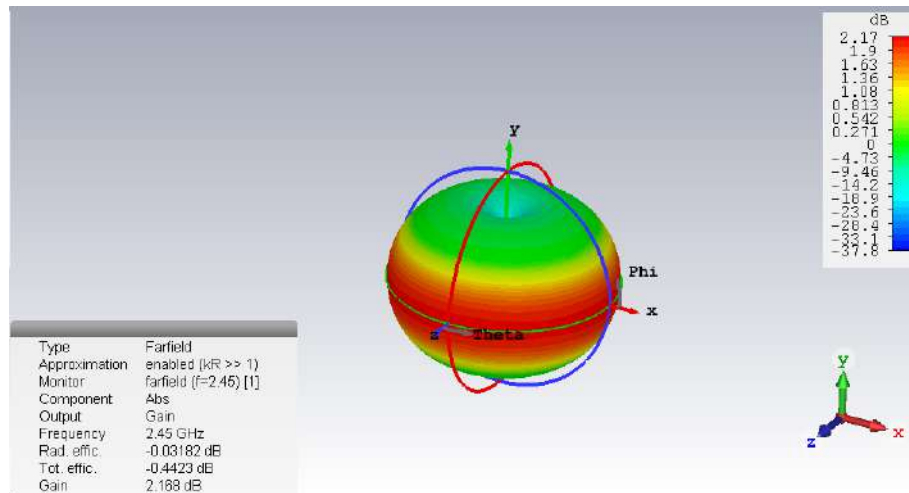


Figure 2.4: The gain of a dipole antenna operating at 2.4 GHz.

The gain one of the most important parameters of an antenna. It is used because it combines the directivity and the efficiency of an antenna.

2.2.7 Field Regions

The immediate surroundings of an antenna can be divided in three distinct fields. The closest one is the reactive near field where the electric and magnetic field are reactive. This means that the electric and magnetic fields are out of phase with each other. The middle field is the radiating near field where the radiating fields begin to emerge and the reactive fields are not predominant any more. The last field is the far field where the radiation pattern is not dependent on distance. This means that the radiation pattern stays the same no matter the distance away from the antenna. One can approximate the field regions using Figure 2.5.

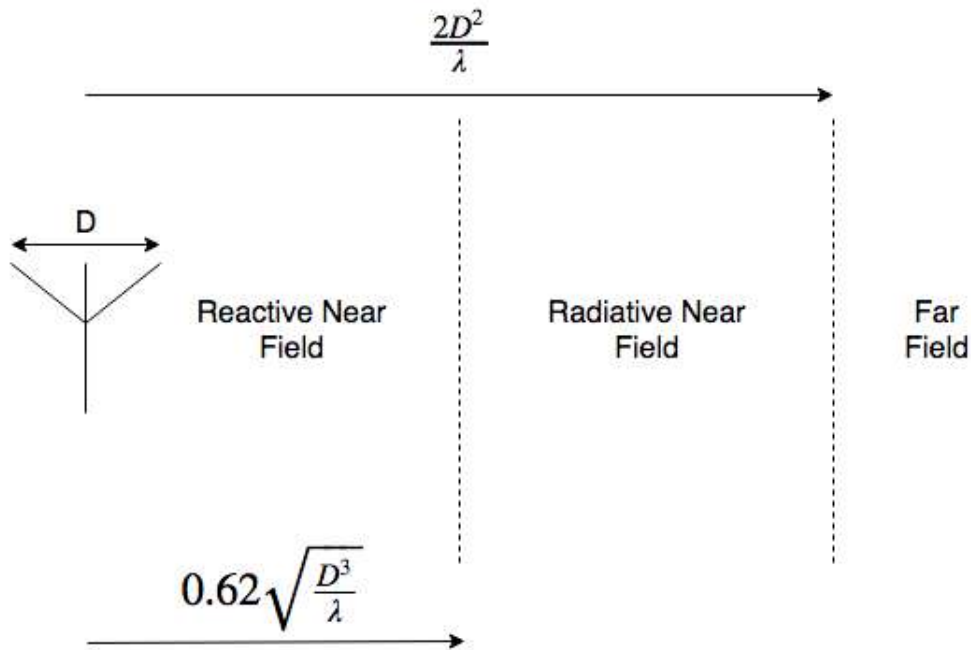


Figure 2.5: Field regions surrounding an antenna.

2.2.8 Bandwidth

Bandwidth is a parameter that describes the frequencies for which an antenna can transmit or receiver power. The bandwidth requirements mostly determine the type of the antenna. For example patch antennas have a very narrow bandwidth while spiral antennas have a wide bandwidth. Table 2.1 shows the bandwidth of several different antennas resonating at the same frequency. [17]

Table 2.1: Bandwidth of 4 different antennas

Antenna	Center Frequency	Frequency Range	Percentage Bandwidth
Patch	1000 MHz	985-1015 MHz	3%
Dipole	1000 MHz	960-1040 MHz	8%
Horn	1000 MHz	154-1848 MHz	169.4%
Spiral	1000 MHz	95-1900 MHz	180.5%

2.2.9 Input impedance

The antenna impedance relates the ratio of voltage and current for a specific frequency at the input of the antenna. The real part of the impedance represents the power that is either radiated away or absorbed by the antenna. The imaginary part represents the power that is stored in the near field of the antenna. One way to check if the antenna is matched is by checking the voltage to standing wave ratio. Theoretically the VSWR is always bigger than 1. When VSWR equals to 1, there is no mismatch loss. However having a VSWR of 1 is almost impossible. For example acceptable VSWR in most cases is two. A VSWR of 3 means that 75% of the power will be delivered to the antenna while a VSWR of 2 means that 90% of the power will be delivered to the antenna [17].

The input impedance of a dipole antenna operating at 2.4 GHz is shown in Figure 2.6.

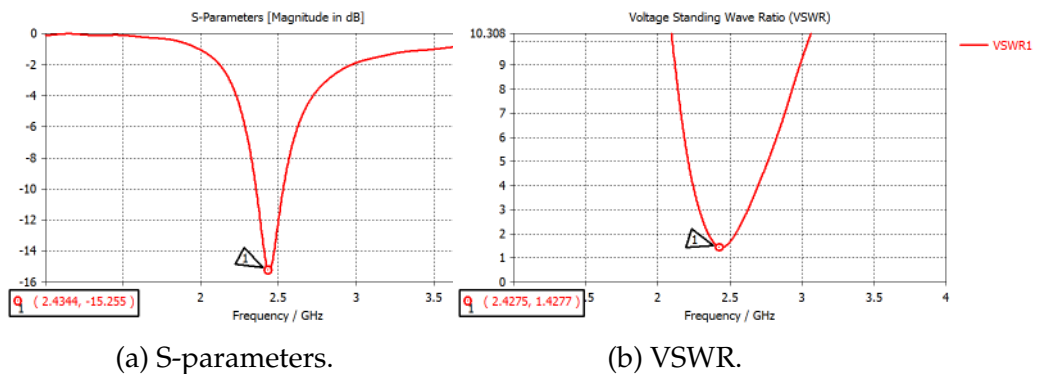


Figure 2.6: Input impedance of a dipole operating at 2.4 GHz.

2.2.10 Coupling

Coupling or mutual coupling between antennas is the absorption of energy from an antenna by another antenna in close proximity. This means that power radiated from one antenna would be captured by another antenna. Similarly, power that could have been captured by one antenna is instead captured by another antenna in close proximity. Therefore, mutual coupling could potentially reduce the performance of the antennas in question.

2.2.11 Antenna Isolation

There are a few ways to isolate mutually coupled antennas. The first way is to increase the distance between the two antennas. The second way is to use a different polarization for the two antennas. Another way of isolating antennas is by designing them to operate at different frequencies. Filtering out the undesired frequency is a way of isolating them even further. Lastly, isolation can be achieved by reducing the correlation coefficient between the antenna's radiation patterns.

2.2.12 Polarization

There are three different kinds of polarization. Specifically there is linear polarization, circular polarization and elliptical polarization. Linear polarization can be either horizontal or vertical polarization. Circular polarization can be either left hand circular polarization either right hand circular polarization. An electromagnetic wave can be achieved by having an electric field and magnetic field varying in orthogonal planes.

Linear Polarization

For a linear polarization to be achieved, the electric field must be varying along a line in a plane. Depending on how the varying electric field is positioned in respect to the earth, it can be either horizontally or vertically polarized.

Circular Polarization

For a circular polarization to be achieved, the electric field must have two perpendicular components. Those components must have the same magnitude. In addition, the orthogonal components must be 90 degrees out of phase.

Elliptical Polarization

Elliptical polarization can be achieved when the two perpendicular components of the electric field have a different magnitude. This can be described by the axial ratio. The axial ratio represents the ratio between the major and minor amplitudes. An axial ration of 1 means that the elliptical polarized wave is a circularly polarized one instead.

Elliptically polarized waves can be considered circular when the axial ratio is less than 3.

2.3 Patch Antennas

The antenna elements that must be considered for this project must be small relative to the operating wavelength. Specifically in order to achieve the goal of the thesis, each antenna element must have a size of approximately $3 \times 3 \text{ cm}^2$. Most antennas have a size relative to that of the wavelength of the operational frequency and therefore careful consideration must be taken when choosing antennas. In addition the antennas must be easy to manufacture and relatively inexpensive.

Antennas that have these properties are patch antennas. They are low profile, conformable to planar and nonplanar surfaces, simple and inexpensive to manufacture using modern printed-circuit technology. However patch antennas do not come without disadvantages. Their efficiency, bandwidth and power is low [4].

2.3.1 Working Principle

The typical patch antenna is consisted of two highly conductive metals. The two metals are called the strip or patch and the ground plane. They are separated by a dielectric material or otherwise known as substrate. Figure 2.7 depicts the side view of a rectangular patch antenna.

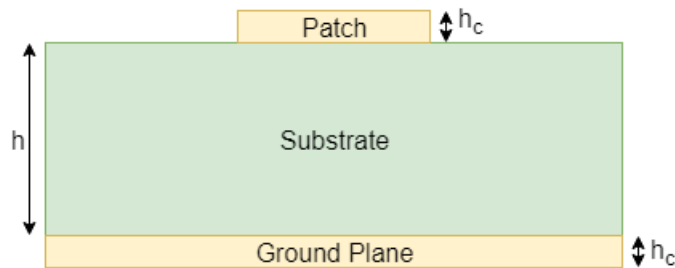


Figure 2.7: Side view of a patch antenna.

One cannot understand how a patch antenna works without understanding what the fringing fields are. Consider Figure 2.8.

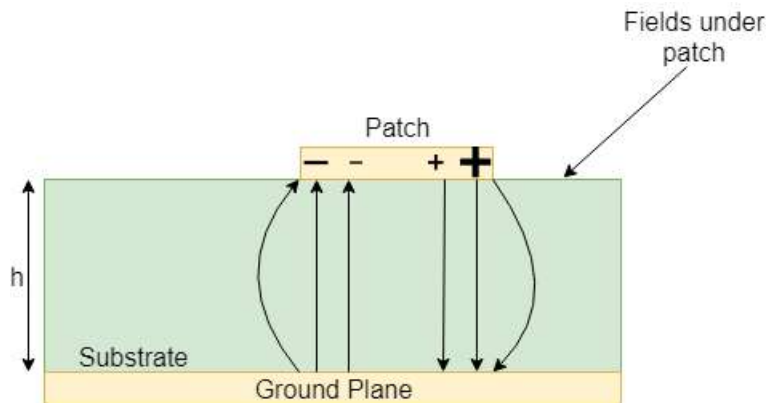


Figure 2.8: Side view of a patch antenna with electric fields in the substrate.

The current at the beginning and the end of the patch is zero. Theoretically the current is maximum at the center, which explains why the impedance is low or high when the antenna is fed either at the beginning or the end respectively. In addition, the antenna is essentially an open circuited transmission line which means that the voltage reflection coefficient will equal to one. This means that the current will be out of phase in respect to the voltage. Therefore at the end of the patch there will be a maximum voltage while at the beginning of the patch the voltage will be minimum. This explains how the fields are created underneath the patch as in Figure 2.8. In addition there will be created additional fields around the edges called **fringing fields** [17].

The fringing fields are responsible for the radiation of the patch antennas. They are created from the advantageous voltage distribution and add up in phase which produces radiation.

It is interesting to notice that the dielectric constant (ϵ_r) plays a huge role in the bending of the fringing fields. A high (ϵ_r) will tighten the fringing fields and will result in less radiation while a low (ϵ_r) will extend the fringing fields away from the patch resulting in a better radiation.

According to the BLE standards the frequencies at which BLE will be used are 2.402, 2.426 and 2.48 GHz [20]. The worst operating frequency to work with according to [21] is channel 38 which corresponds to 2.426 GHz. This makes the antenna design easier to implement because the patch antennas have a very narrow bandwidth. The substrate that used is FR-4 which has a dielectric constant of 4.4.

The two most widely used methods for feeding an antenna are the

microstrip line and the coaxial probe. Apart from being widely used they are also easy to fabricate and simple to match. In most cases matching for a microstrip line is performed by controlling the width of the feed line and the length of the slot. In order to match a coaxial feed controlling the feed position will provide proper matching [4].

Apart from arbitrary geometrical shaped patch antennas other types of antennas can also be used as thin strip conductors printed on the surface of a substrate. These include the dipole, the monopole, the inverted-F and planar inverted-F antennas.

2.4 Substrate

The substrate is a laminated material commonly used in printed circuit boards. It is mostly used as a layer between the radiating part and the ground plane of an microstrip patch antenna

The substrate is not only providing robustness to the antenna but allows surface waves to propagate in the substrate. This in turn causes the fields at the end of the patch to undergo fringing. The amount of fringing depends on the substrate's height and dimensions. Therefore in order to account for the fringing effects which are partially dependent on the dimensions the effective dielectric constant was introduced [22]. Equation 2.5 describes the effective dielectric constant (ϵ_{eff}):

$$\epsilon_{eff} = \frac{\epsilon_r + 1}{2} + \frac{\epsilon_r - 1}{2} \left[1 + 12 \frac{h}{W} \right]^{1/2} \quad (2.5)$$

The substrate is characterized by three parameters, the height (h), the dielectric constant (ϵ_r or Dk) and the loss tangent (δ or Dk). In study [23] there have been simulations on patch antennas using different substrate materials while keeping the same resonant frequency. Table 2.2 shows their results.

Parameter	Bakelit	FR-4 Glass Epoxy	RO4003	Taconi TLC	RT Duroid
Resonant Frequency	8 GHz	8 GHz	8 GHz	8 GHz	8 GHz
Dielectric Constant	4.78	4.36	3.4	3.2	2.2
Loss Tangent	0.03045	0.013	0.002	0.002	0.0004
Size	9.15 mm	9.575 mm	10.85 mm	11.75 mm	13.475 mm
Return Loss	-18.11 dB	-16.14 dB	-14.75 dB	-14.39 dB	-20.99 dB
Gain	3 dBi	4 dBi	5 dBi	5.5 dBi	6.5 dBi
Bandwidth	12.5%	10.12%	7.59%	8.8%	15%
Radiating Efficiency	45%	50%	70%	67.5%	80%

Table 2.2: Impact of different substrates.

The properties of five similar antennas varying in patch size and dielectric material are presented. They are all matched to resonate at 8 GHz. Firstly, the size is inversely proportional to the dielectric constant. The Bakelit antenna has the smallest size because it has the highest dielectric constant. The gain and the bandwidth are mostly dependent on the loss tangent. In the end the highest the loss tangent, the lower the radiating efficiency will be. Therefore it is important to specify the needs of the antenna and choose a substrate accordingly. For example in the need of a high gain low size antenna, a dielectric with a high dielectric constant and a low loss tangent is desirable.

An important aspect not been taken into to consideration is the height of the substrate. Additional information regarding this matter can be found in [22].

2.5 Path Loss Model

One of the most fundamental equations in antenna theory is the **Friis Transmission Equation**. It calculates an antenna's received power, while another antenna is transmitting. The equation takes into consideration the gains of the receiving antenna (G_r) and transmitting antenna (G_t), the distance separating the antennas (R), the total power received (P_r) and transmitted (P_t). It must be noted that this is true for propagation in the a free-space medium. The **Friis Transmission Equation** can be seen in Equation 2.6.

$$\frac{P_r}{P_t} = \left(\frac{\lambda}{4\pi R}\right)^\alpha G_t G_r \quad (2.6)$$

which in dB translates to,

$$P_r - P_t = G_t + G_r + \alpha * 10 \log_{10}\left(\frac{\lambda}{4\pi R}\right) \quad (2.7)$$

which means that the gain of the receiving antenna should be,

$$G_r = P_r - P_t - G_t - \alpha * 10 \log_{10}\left(\frac{\lambda}{4\pi R}\right) \quad (2.8)$$

The **Friis Transmission Equation** can be used as a general rule. It shows how the frequency and the distance between antennas affect the power received on an antenna. Therefore it is seen that the power received by an antenna is inversely proportional to the operational frequency of the antennas and the distance between them.

The equipment available is sensitive to -127 dB according to [24]. The gain of the antenna is shown to go from 1.1 dBi to 3.3 dBi in [25]. However, dBi is used for directivity. Therefore, there is not sufficient knowledge about the gain of this antenna. We can assume that since the antenna is of a IFA type antenna and the length is similar to most commercially used antennas, the gain should be around -6 dB.

According to Equation 2.6, [26] and [25], [27] the following model was created where,

$$\begin{aligned} \lambda &= 123mm \\ G_t &= -6dB \\ P_r &= -127dB \\ P_t &= -30dB \\ R &= 1000mm \\ \alpha &= 3 \end{aligned}$$

Figure 2.9 shows the dependence of the gain requirements of the antenna receiver versus the distance of the transmitting antenna. In this thesis, the maximum distance that the tests were conducted was 1 meter. This is of the essence, as the receiver antennas gain requirements are extremely low which causes the efficiency to be unimportant in this project.

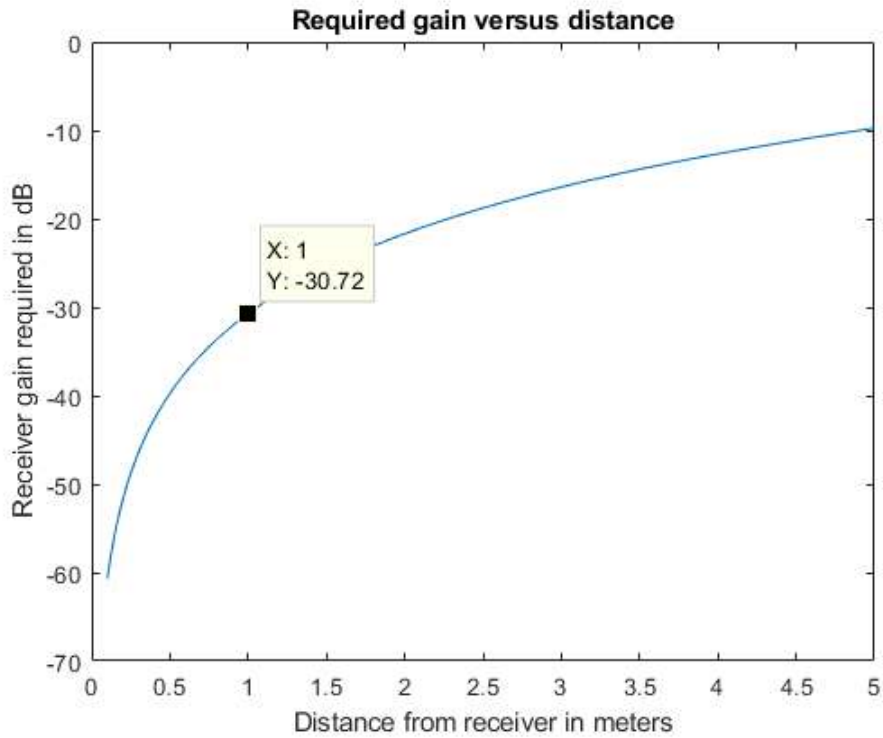


Figure 2.9: Receiving antenna gain requirement

In the thesis proposal the system should work efficiently in the maximum range of one meter. This corresponds to a receiving antenna gain of -30.72 dB.

2.6 Angle of Arrival

There have been a lot of studies for Angle of Arrival (AoA) or otherwise known as Direction of Arrival (DoA) [28] [5] [4].

Essentially the AoA algorithms determine the direction of an incoming signal by calculating the time delay between different antenna elements. Considering the most basic approach two antenna elements are spaced at a distance d . The antenna elements are considered to be dimensionless isotropic antennas. Consider Figure 2.10.

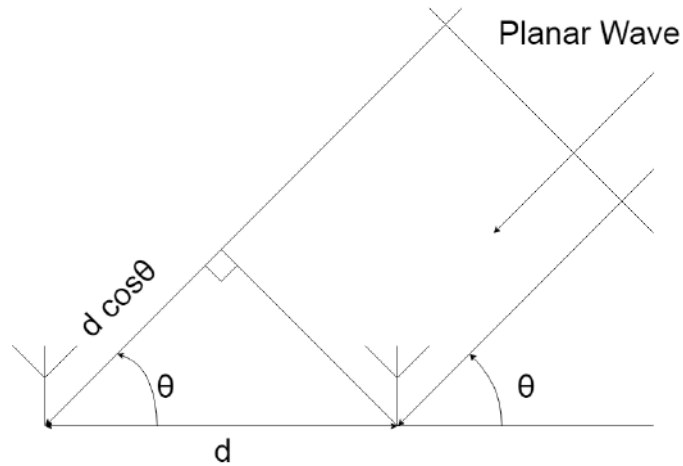


Figure 2.10: Two antenna elements and an incoming planar wave.

The wave arrives at an angle of 45° in respect to the reference line between the two antennas. The wave arrives to the two elements at different times and the time delay is

$$\Delta t = (t_1 - t_2) = \frac{\Delta d}{v_0} = \frac{d \cos \theta}{v_0} \quad (2.9)$$

Solving for θ

$$\theta = \cos^{-1}\left(\frac{d}{v_0} \Delta t\right) = \cos^{-1}\left(\frac{d}{v_0} (t_1 - t_2)\right) \quad (2.10)$$

The above algorithm works great for angles for calculating the angles from one side of the reference line. However, when the signal arrives from the other side of the reference line the algorithm cannot distinguish which side of the reference line is the signal coming from. The reason for this is that the time required for both signals to pass through both antennas will be the same.

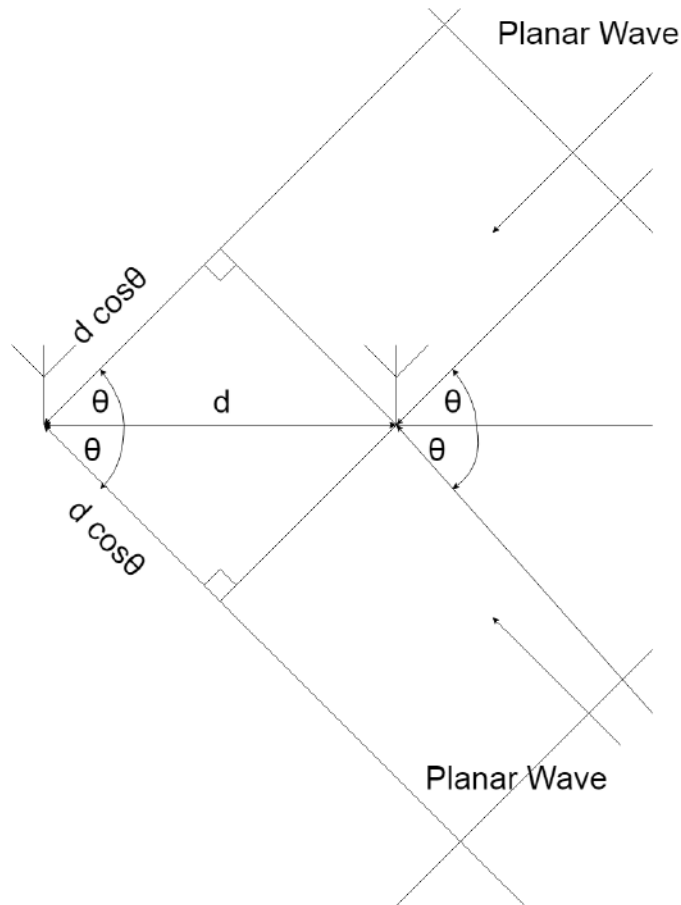


Figure 2.11: Two antenna elements and two incoming planar waves.

2.7 Bluetooth Low Energy Standards

Bluetooth is a protocol used by devices to communicate wirelessly. The operating channels that the new proposal implements are shown in Table 2.3.

RF channel	Channel Index	Center Frequency (MHz)
0	37	2402
12	38	2426
39	39	2480

Table 2.3: Advertising channel center frequencies

The author of [21] has done research on the Bluetooth Low Energy Standards. What is important for this project is that the reader has a good understanding of the operating channels. For more information on the BLE proposal refer to [21].

2.8 Evaluation Method

The evaluation of the Angle of Arrival using pure interferometry has been investigated in [21]. However, it is important to contain here some essential information about the evaluation of the system.

2.8.1 IQ Sampling

As we have already discussed in 2.6, the angle of an incoming wave can be calculated by measuring the time it requires the signal to pass from antenna 1 to antenna 2. However, the system that the evaluation is being studied upon can calculate In-Phase and Quadrature component data (IQ data) instead of the time difference. The IQ data consists of two components, the I which is the momentarily value while the Q component is the value that is delayed by $\pi/2$.

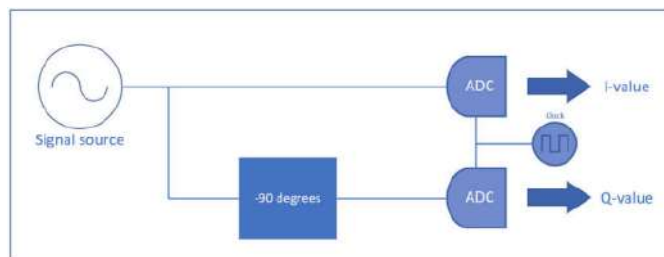


Figure 2.12: IQ sampling scheme.

2.8.2 Time to Phase

In this section algorithm for transforming the time difference into phase difference will be explained.

As explained in 2.6, in order to calculate the Angle of Arrival, two variables are needed, the distance between the antenna receivers and the time difference of the electromagnetic wave to pass through the

antenna receivers. distance is known as it depends on the arrangement of the antennas, while the time difference must be calculated.

The time difference equals to the time per phase unit multiplied by the phase difference.

$$\theta = \cos^{-1} \left[\frac{v_0}{d} * \frac{1}{2\pi * f} * \Delta\varphi \right] = \cos^{-1} \left[\frac{\Delta\varphi * \lambda}{2\pi * d} \right] \quad (2.11)$$

This equation shows how the Angle of Arrival can be calculated from the the phase difference. The general scheme for calculating the Angle of Arrival can be seen in 2.11. However, because of the indicators that the equipment had the expression for calculating the Angle of Arrival has been changed to:

$$\theta = \sin^{-1} \left[\frac{\Delta\varphi * \lambda}{2\pi * d} \right] \quad (2.12)$$

2.8.3 Phase Difference Calculation

There have been several methods for calculating the phase difference using IQ samples. For more information about the different methods refer to [21]. The method used is called "four-quadrant inverse tangent" and the phase is calculated as:

$$\Delta\varphi = \arctan2 \left((I_1 + Q_1 i) * (I_2 + (-1 * Q_2) i) \right) \quad (2.13)$$

The reason for this choice of method is that there are combinations of phases that could potentially yield wrong phase differences. Figure 2.13 shows that using this method the calculated phase difference is the same as true phase difference independent of the phase of the reference signal.

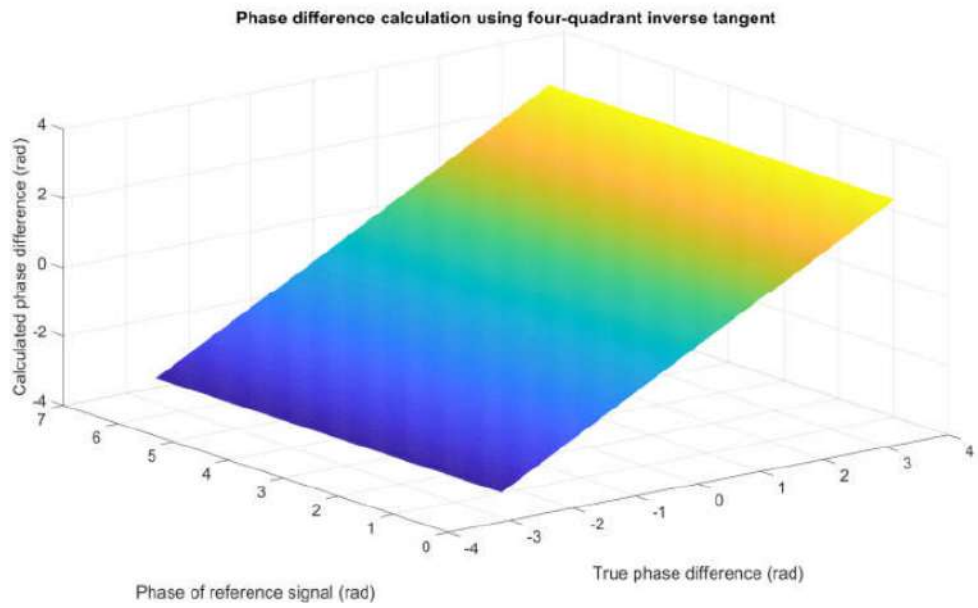


Figure 2.13: Phase difference calculation using four-quadrant inverse tangent.

Chapter 3

Challenges for AoA Antenna Solution

In theory an AoA solution is quite simple to achieve as discussed in Section 2.6. However, the theory is not compensating for problems in real life. Some of the major challenges are discussed in the following sections.

3.1 Orientation and polarization

The orientation and subsequently the polarization of the antenna plays a huge role in the efficiency of the system. As discussed in 2.2.12, antennas are either vertically, horizontally, right-handed or left-handed circularly, or elliptically polarized.

In practice this means that the orientation of the transmitter and the receiver plays a huge role in power. Theoretically by transmitting a vertically polarized electromagnetic wave in the direction of a horizontally polarized receiver, the receiver would get no power. Table 3.1 shows the amount of gain reduction when the transmitter and the receiver are using a different polarization [29].

Tx Antenna Polarization	Rx Antenna Polarization	Ratio of Power Received to Maximum Power			
		Theoretical		Practical	
Vertical	Vertical	0 dB	1	*	*
Vertical	Slant (45° or 135°)	-3 dB	1/2	*	*
Vertical	Horizontal	-∞ dB	0	-20 dB	1/100
Vertical	Circular (right-hand or left-hand)	-3 dB	1/2	*	*
Horizontal	Horizontal	0 dB	1	*	*
Horizontal	Slant (45° or 135°)	-3 dB	1/2	*	*
Horizontal	Circular (right-hand or left-hand)	-3 dB	1/2	*	*
Circular (right-hand)	Circular (right-hand)	0 dB	1	*	*
Circular (right-hand)	Circular (left-hand)	-∞ dB	0	-20 dB	1/100
Circular (right-hand or left-hand)	Slant (45° or 135°)	-3 dB	1/2	*	*

Table 3.1: Impact of different polarization between transmitter and receiver

3.2 AoA Antenna Switching Board Matching

The AoA Antenna Switching Board is not perfectly matched to 50 Ohm. This means that even with perfectly matched antenna elements some power would be reradiated. The impedance of the switching board during sampling and termination is shown in Figure 3.1 and 3.2. In addition, the ports are unbalanced.

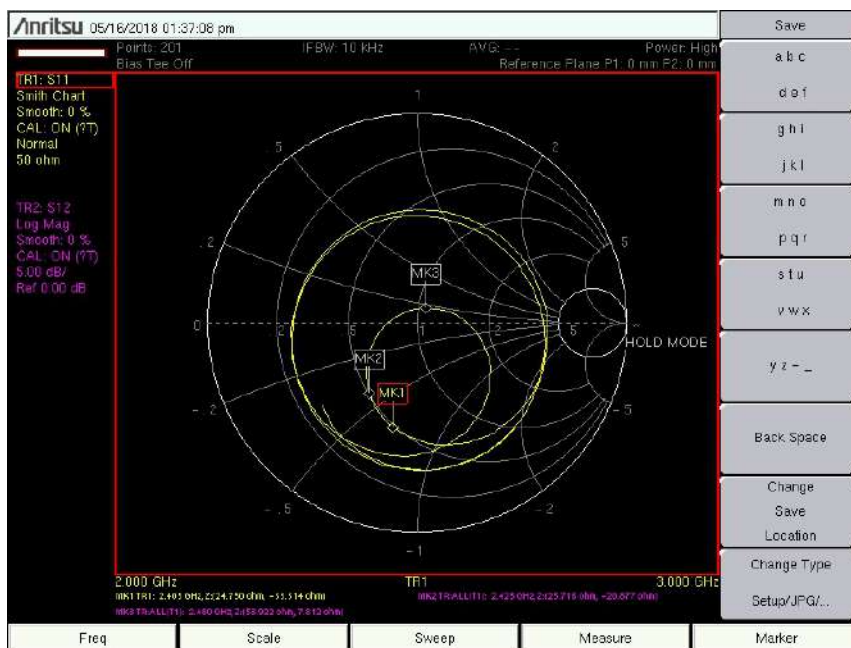


Figure 3.1: Switching board during sampling.

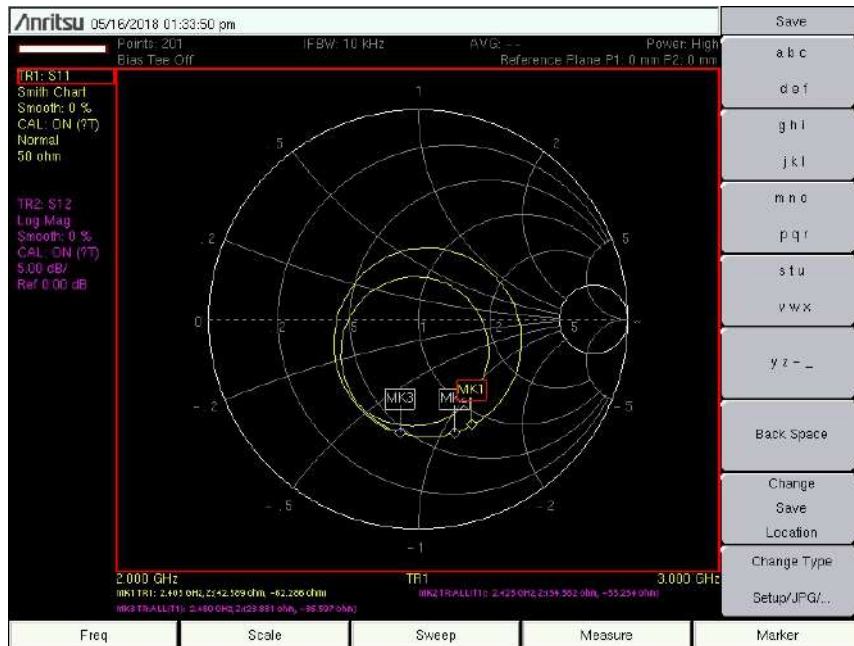


Figure 3.2: Switching board during termination.

3.3 Coupling

Antenna elements that are in close proximity from each other provide interference with each other as discussed in Section 2.2.10. A way of combating coupling is by using antenna elements that do not reradiate energy towards the antenna elements of close proximity. Omnidirectional antenna elements are not desirable because reradiated electromagnetic waves would interfere with original electromagnetic waves and would create interference.

However by implementing extremely accurate impedance matching, reradiated waves would not exist because all of the power would be absorbed by the antenna elements. Another way of combating coupling is by implementing antenna isolation as discussed in 2.2.11.

3.4 Reflections

Reflections from walls, floors, ceiling and equipment could alter the phases that the antenna array is receiving. This could potentially, result in false angle measured.

3.5 Distance

Distance is inversely proportional to power. In other words the bigger the distance the lower the power. The **Friis Transmission Equation** 2.6 explains this.

3.6 Interference

Interference from another source can be either constructive or destructive. The signals from different sources will add or subtract in magnitude and therefore will provide wrong estimations when the phase difference is calculated.

3.7 Size

The size of the final design constricts the dimensions of the antenna elements in question. Size is playing a big role in the directivity of the antenna element. The smaller the antenna element the less directivity it has.

3.8 Phase Center

The phase center of an antenna is the point where its phase front originates. Specifically, any point on the EM wave that is in the same sphere has the same phase. However, this point is dependent on the direction of an incoming RF wave. Therefore, in some cases the incoming wave can disturb the phase center of the antenna and provide wrong phases. In addition, the phase center is a property that is extremely difficult to calculate [30].

Chapter 4

Antenna Design

In this chapter focus will be drawn to the antenna design of several antennas. Firstly, we need to specify the requirements for the antennas. The biggest concern is that the antennas are small enough that they can be fitted on a door lock. Texas Instruments used a dipole in order to avoid coupling in an AoA application. Information about those antennas can be found in [31]. In addition, they explain that the phase center is always at the feeding point in the middle of the antenna, regardless of the direction of the incoming RF wave. It also does not receive or transmit RF power in the direction of its own axis. This means that if we place them side by side, they will interfere minimally with each other.

However, the main problem that they argue is that dipole antennas are fully differential, and must be fed with a balanced signal away from ground planes. If the ground plane is too close, it will effectively short circuit the antenna as the wave reflected by the ground plane is the inverse of the incoming wave. If it is further away, it will reflect RF power back out to the antenna.

Their solution to this problem is the use of a corrugated ground plane. In order to avoid out of phase reflections, the ground plane has to be in close proximity to the antenna. However, this would short circuit the antenna. The corrugated ground plane removes the boundary current by forcing it to take a detour of 180 degrees per finger, so each segment cancels the effect of the neighboring segments. Net effect is zero current and an in-phase reflection.

Therefore, they recommend that the antennas used should not rera-diate in the direction of other antennas and adding a ground plane

which does not reflect out of phase electromagnetic waves.

Texas Instruments have tested two different types of antennas in the receiver. The first type is a chip antenna. They tested different designs of chip antennas but were unable to extract satisfactory results. The other type was a dipole antenna. The former paragraphs explain the reason for their choice. However, the system is not using only AoA. It actually uses RSSI to distinguish which antenna array receives the highest power, and then the AoA is measured on that antenna array.

Taken into account all of the above and the requirements of the project I chose the circularly polarized patch antenna as the antenna to be made. It does not reradiate towards the other antenna elements and it is more versable with credential orientation. However the gain and efficiency will be very low because of the different polarization of the credential. In addition if the polarization of the antenna elements is different we expect a big decrease in the coupling between them.

4.1 Square Ring Meandered Antenna

A small size patch antenna is proposed in [32]. This antenna design is relatively small compared to other patch antenna types. In addition this particular antenna is single fed in contrast to most CP antenna designs which require two feeding ports.

4.1.1 Simulation

The antenna is consisted of a copper ground plane and a meandered copper patch which is separated from the ground plane by a 0.4mm thin FR-4 substrate. The antenna is using a microstrip feeding line because it is easier to place it on different surfaces instead of a SMA probe. Figure 4.1 shows the dimensions of the antenna. The antenna dimensions are extremely small with comparison to other antenna designs being 24 mm wide and 24 mm long while the height is 0.4 mm. This makes the antenna extremely low profile which results in a lot of potential uses.

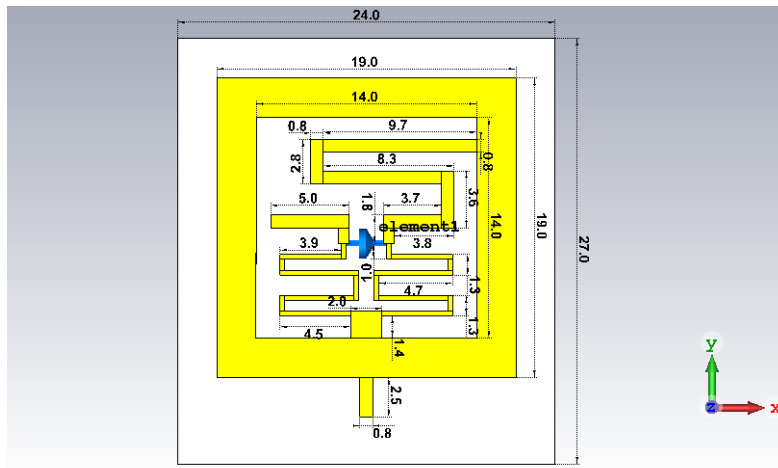


Figure 4.1: Dimensions of the Square Ring Meandered Antenna.

The antenna that emerged from the simulation shows similarities with the proposed design. The return loss S_{11} can be shown in Figure 4.2. Clearly the return loss coefficient ensures less than 1% power reflection for all desired frequencies. In addition it also ensure less than 10% power reflection for more than 200 MHz bandwidth. This ensures that the antenna is not sensitive to detuning due to different materials its vicinity.

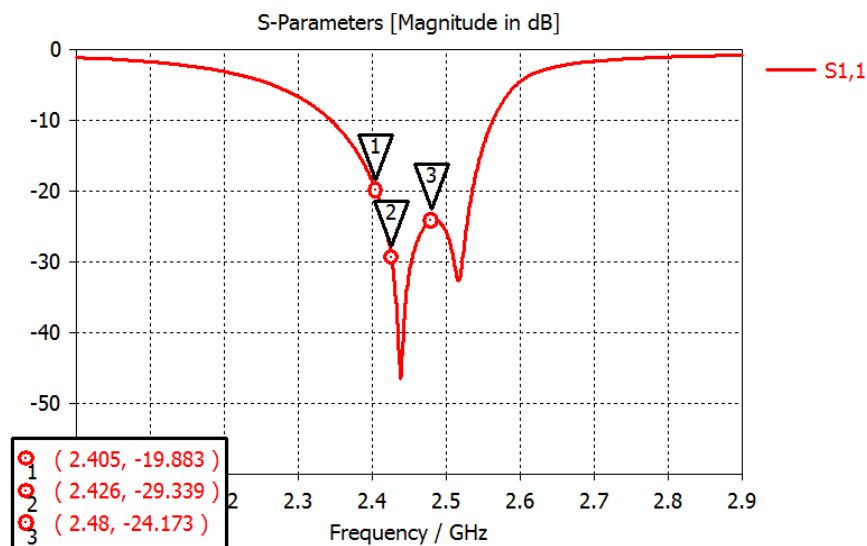


Figure 4.2: S_{11} parameters of the Square Ring Meandered Antenna.

Lastly, the gain of the antenna is shown in Figure 4.3. The designer

of this antenna did not give the gain measurements and it is shown that it varies between -21.2dB and -27.35dB .

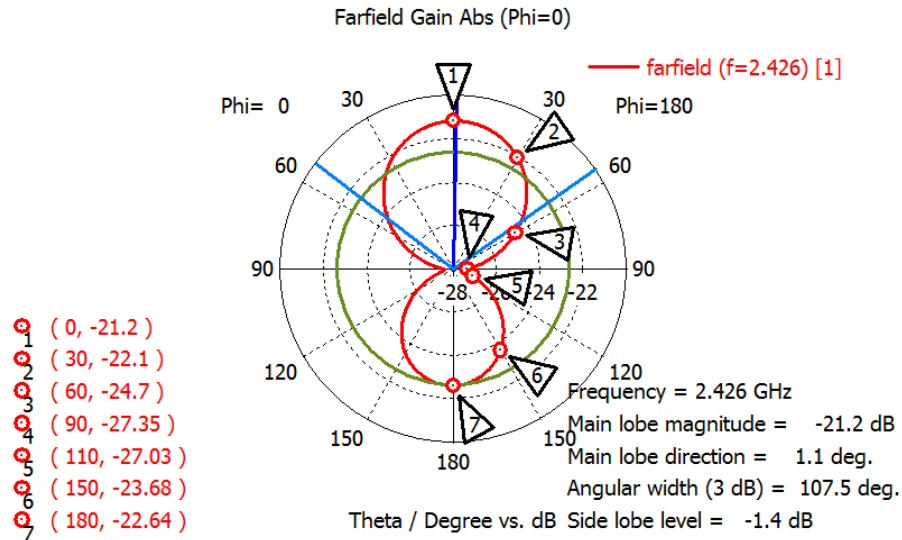


Figure 4.3: Gain parameters of the Square Ring Meandered Antenna.

In addition, the axial ratio is shown in Figure 4.4. For the most part the axial ratio is below the 2 dB threshold and the antenna can be considered circularly polarized.

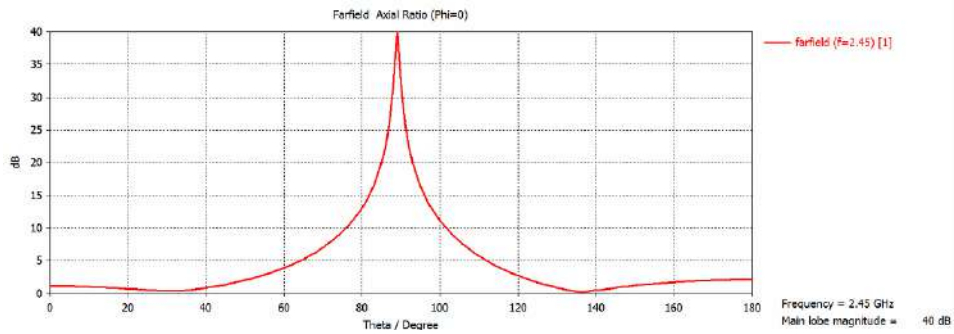


Figure 4.4: Axial ratio of the Square Ring Meandered Antenna.

Finally, the results fit the requirements of the system.

4.1.2 Measurements

The antenna was manufactured using printed circuit technology by photoetching the top layer of the patch antenna in the required design.

The substrate used between the ground plane and the top layer was a 0.4 mm high ISOLA FR-4 dielectric. Figure 4.5 depicts the produced antenna.

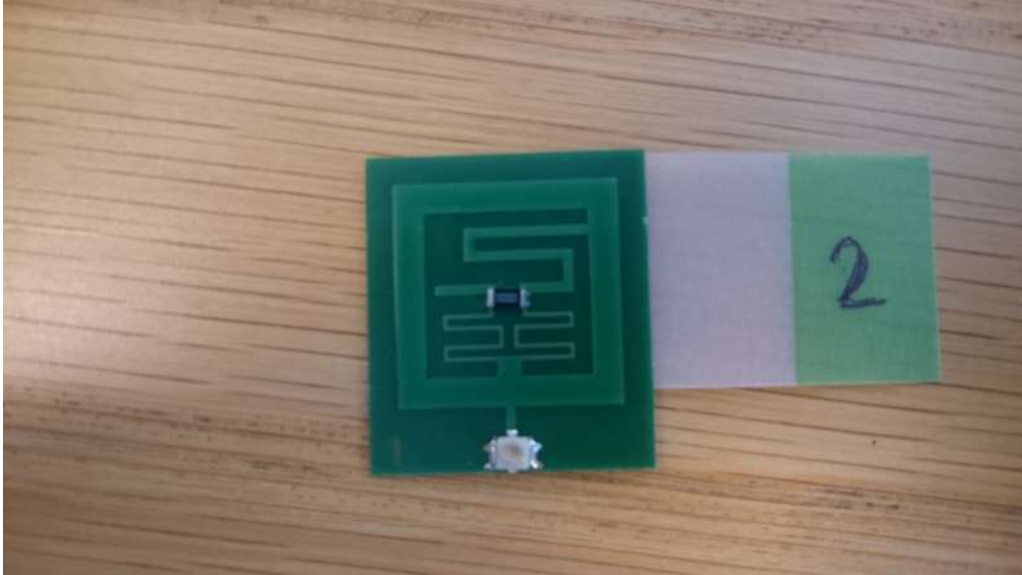


Figure 4.5: Manufactured Square Ring Meandered Antenna.

The following figure shows the S_{11} results of the manufactured design.



Figure 4.6: S_{11} parameters of the Manufactured Square Ring Meandered Antenna.

It is shown that the antenna has a bandwidth of 200 MHz. However the results deviate from the simulation. This is attributed to the manufacturing process which added a liquid photoimageable solder mask. A reader is referred to [33] for more information.

4.2 Normal Patch Antenna

In [34] the authors suggest that by introducing a slot in the patch of a microstrip antenna the resonant frequency is lowered. The introduction of the slot the surface current path is lengthened along the slot parameters. Therefore, the effective resonance length is shortened. This results in a lowered resonant frequency. In other words, slot loading a patch antenna is a potential miniaturization. However, the large accumulation of surface current around the edges of the slot decrease the gain. Therefore, a trade-off between gain and miniaturization must be considered.

4.2.1 Simulation

Figure 4.7 depicts the dimensions of the simulated antenna.

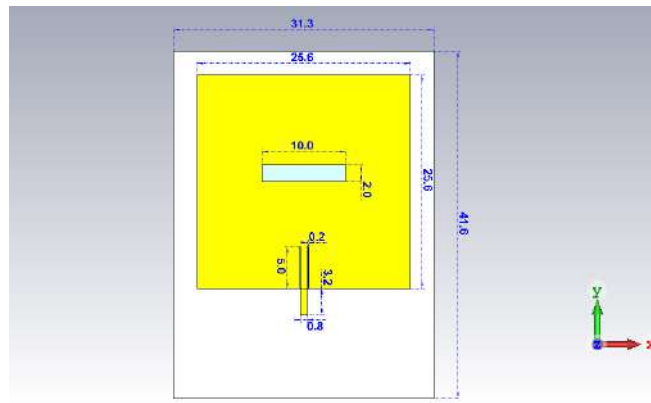


Figure 4.7: Dimensions of the Normal Patch Antenna.

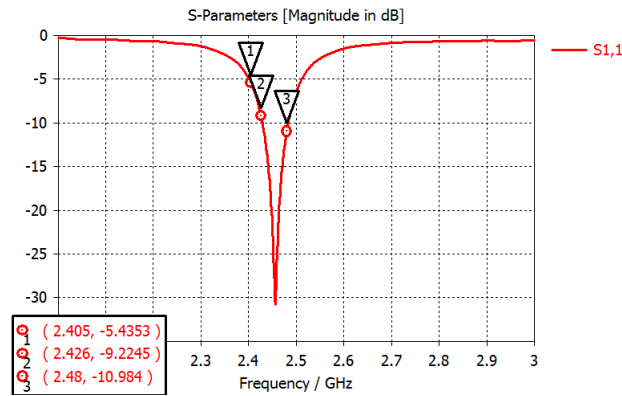


Figure 4.8: The S_{11} parameters of the Normal Patch Antenna.

In Figure 4.8 the return loss coefficient S_{11} parameters are shown. Figure 4.9 shows the gain of the Normal Patch Antenna.

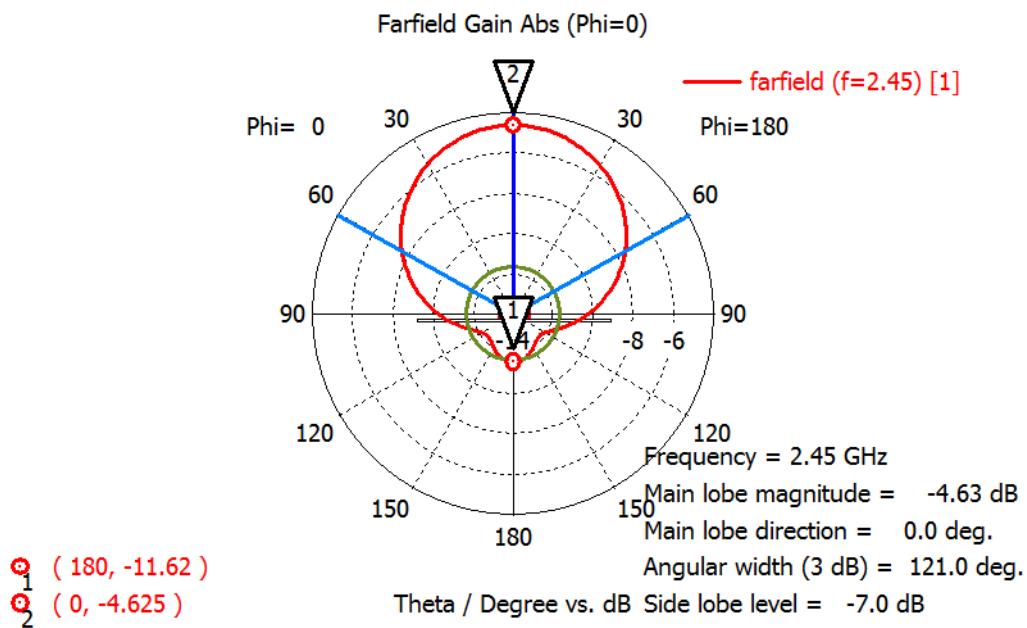


Figure 4.9: Gain of the Normal Patch Antenna.

4.2.2 Measurements

The manufactured antenna is shown in Figure 4.10.



Figure 4.10: Manufactured Normal Patch Antenna.

The measured S_{11} parameters are shown in Figure 4.11.



Figure 4.11: Measured S_{11} parameters of the Normal Patch Antenna.

There is some deviation from the simulated design. The manufactured antenna is mismatched. However, the S_{11} parameters show that for the desired frequency less than 15% of the power will be reflected from the antenna.

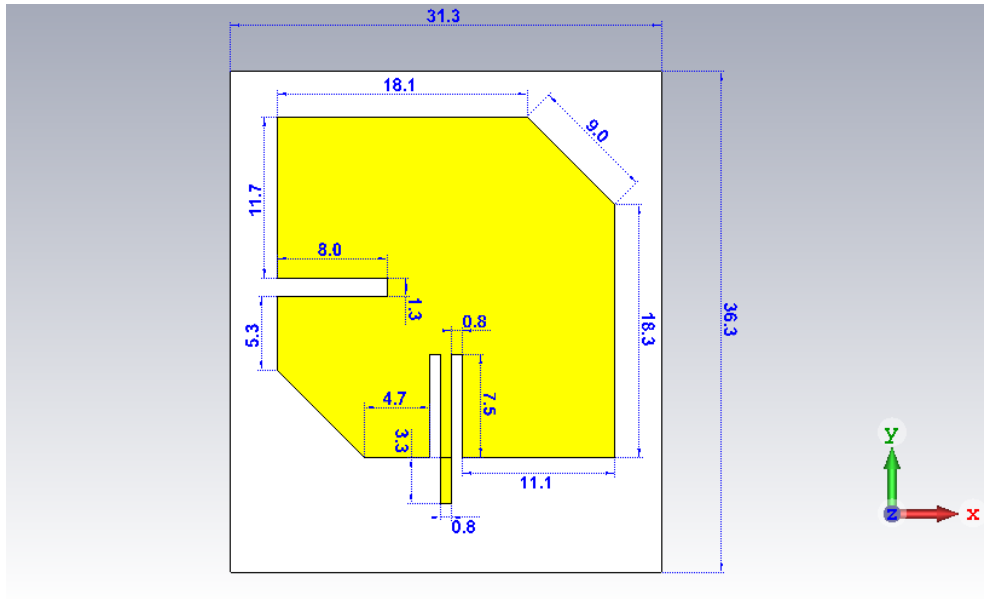
4.3 Circularly Polarized Patch Antenna

Another design was implemented according to [35]. The author proposes a lot of different patch antennas that can achieve circular polarization and discuss each of the properties. In addition he provides ways of achieving miniaturization for these antennas. However, those antennas are made on a 60 mm wide and 60 mm long, 1.6 mm high FR-4 high dielectric.

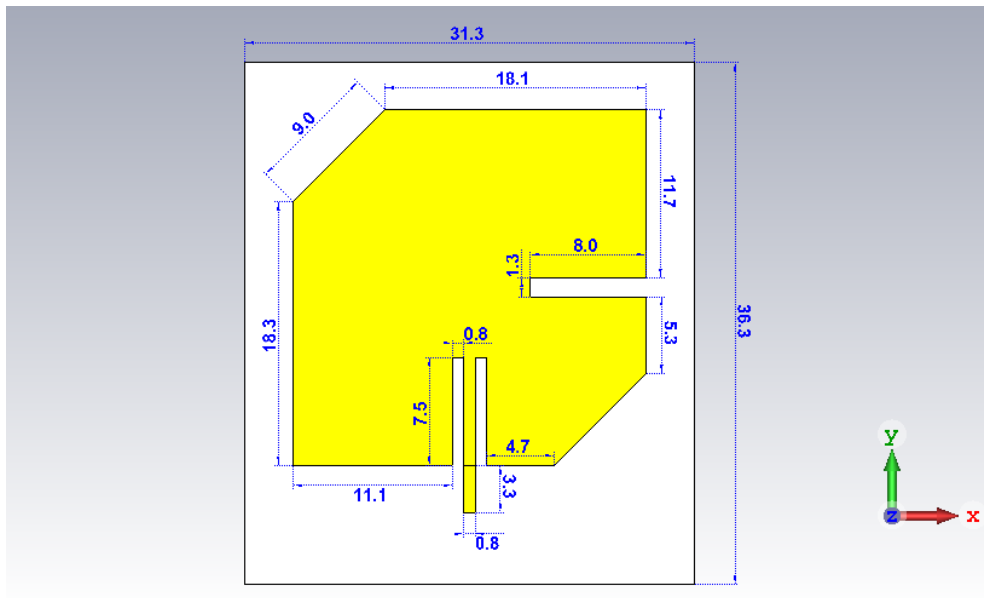
4.3.1 Simulations

For the purpose of this project ground plane size was decreased to fit the requirements to 31.25mm. In addition the patch size was decreased. Two different variations of the design were made based on their polarization. Therefore, two designs each having a right-hand and a left-hand polarization were made. They could be used to reduce the reradiation between them.

Figure 4.12 provides the dimensions of the two designs.



(a) Left-hand CPPA.



(b) Right-hand CPPA.

Figure 4.12: The dimensions of the two circularly polarized patch antennas.

In Figure 4.13 the return loss coefficient S_{11} parameters are shown. It can be seen that the antennas have a bandwidth of more than 100 MHz where the power return loss is 40%. The particular antennas are

quite inefficient. Even though the gain 4.14 shows that they fall under the requirements of the system, the potential reflected waves could interact with the system's accuracy.

The antennas were designed on FR-4 substrate that had a height of 1.6 mm. The antennas were much more efficient and had a much higher gain. However, time did not allow for the manufacturing of these antennas.

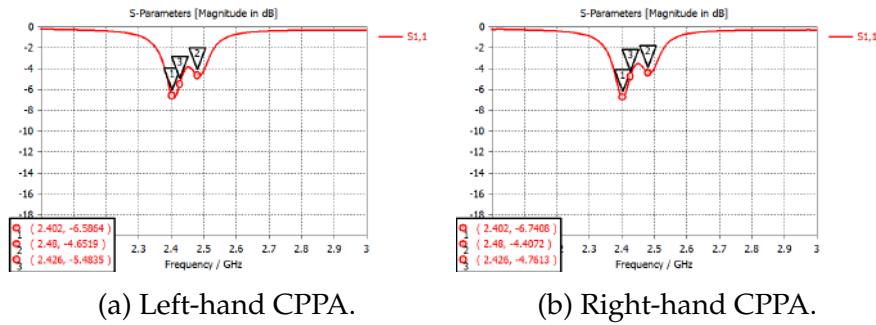
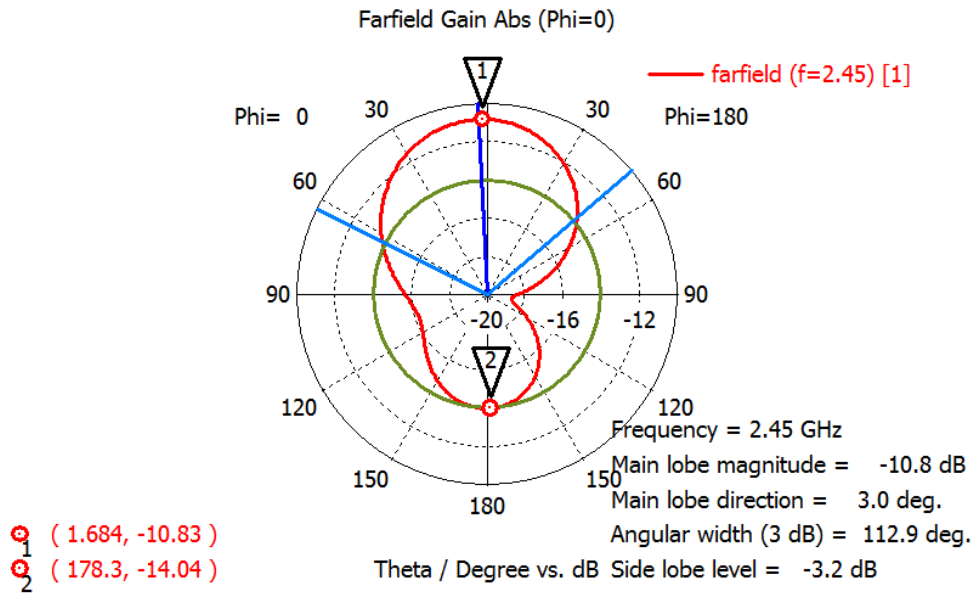
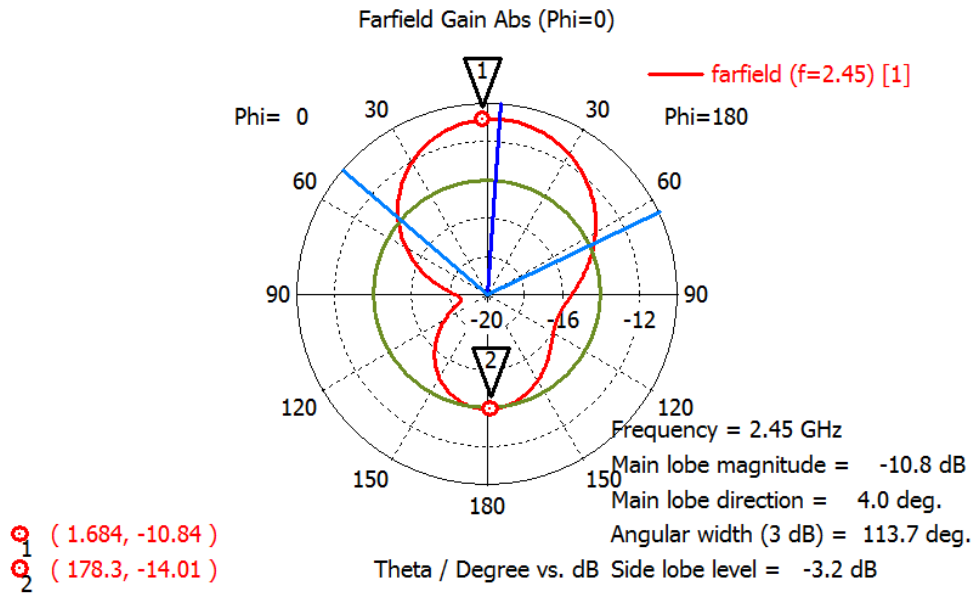


Figure 4.13: The S_{11} parameters of the two circularly polarized patch antennas.



(a) Left-hand CPPA.

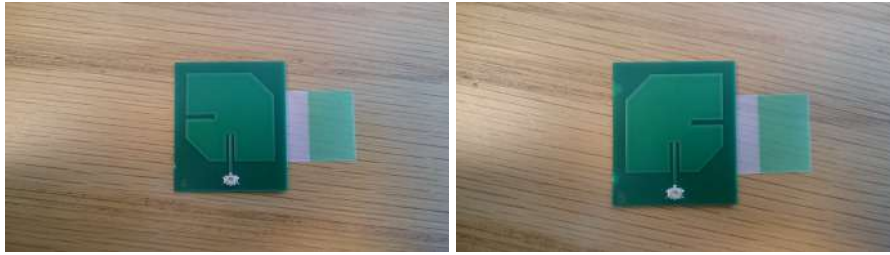


(b) Right-hand CPPA.

Figure 4.14: The gain of the two circularly polarized patch antennas.

4.3.2 Measurements

The manufactured antennas are shown in Figure 4.15.

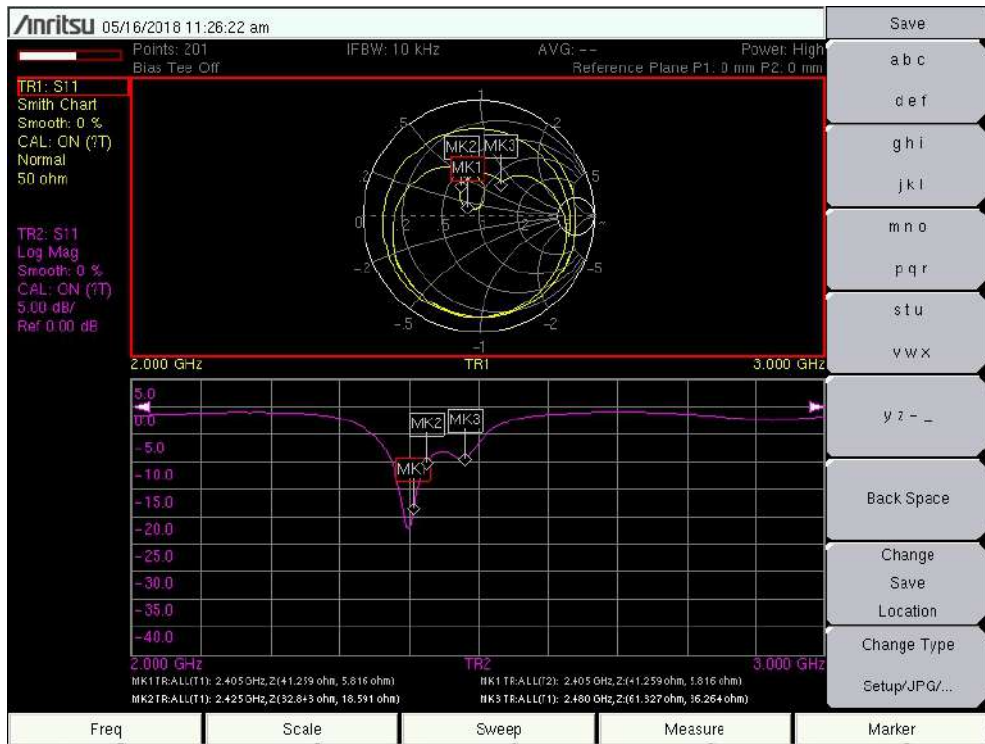


(a) Left-hand CPPA.

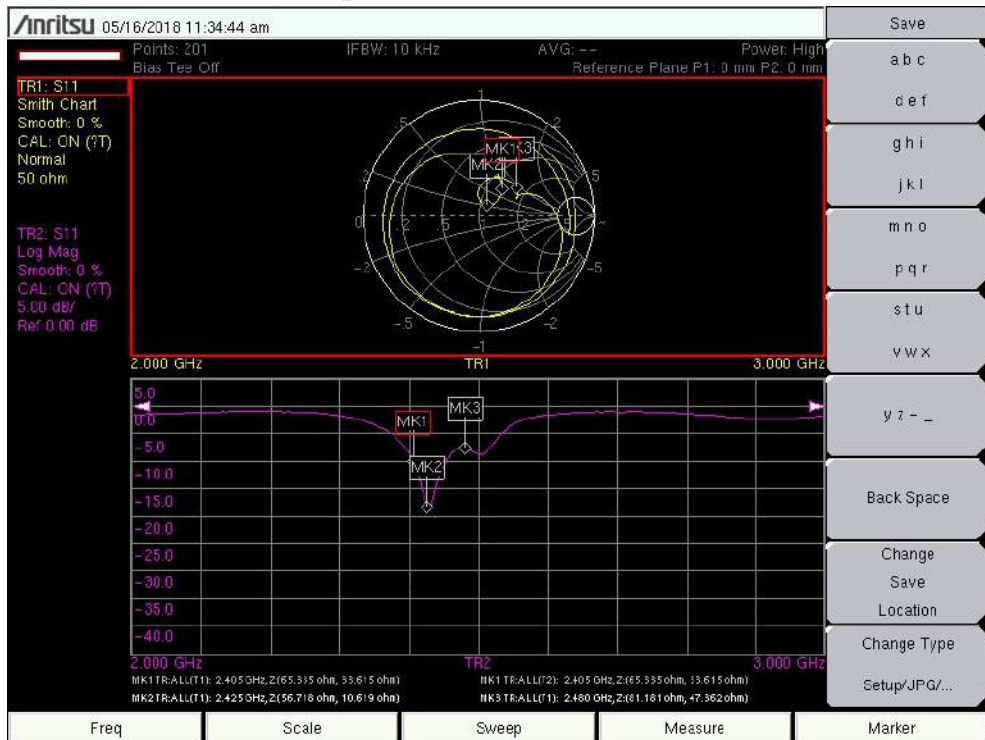
(b) Right-hand CPPA.

Figure 4.15: The manufactured circularly polarized patch antennas.

The measured S_{11} parameters are shown in Figure 4.16.



(a) S_{11} parameters of Left-hand CPPA.



(b) S_{11} parameters of Right-hand CPPA.

Figure 4.16: The S_{11} parameters of the two circularly polarized patch antennas.

The measurements show deviation from the simulation results. This is attributed to the manufacturing process.

4.3.3 Improvement

The antenna parameters can be improved to a significant extent by altering some dimensions. The antennas require a thicker dielectric, such as a 1.6 mm high FR-4.

4.4 Standard Patch Antenna

The standard patch antenna (SPA) is a rectangular patch antenna fed coaxially. The dimensions of can be seen in Figure 4.17. This particular antenna was designed to have a higher gain than the other antennas designed and to be linearly polarized. The feeding point is placed 31.5 mm from the bottom of antenna as shown in Figure 4.17.

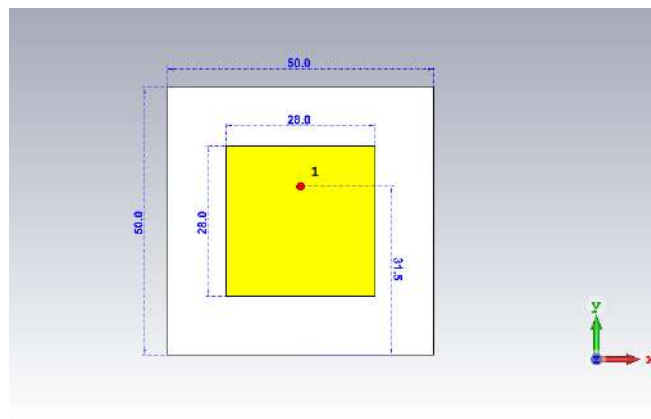


Figure 4.17: The dimensions of the SPA

In Figure 4.18 the S-parameters of the SPA can be seen.

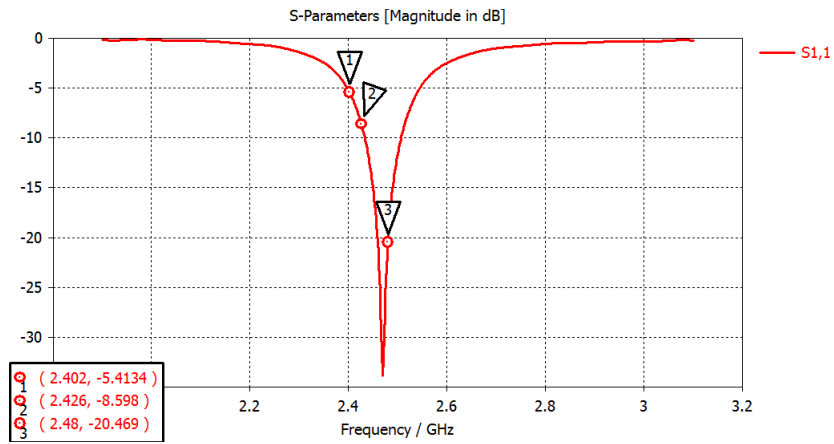


Figure 4.18: The S-parameters of the SPA

Finally the gain of the SPA can be seen in Figure 4.19.

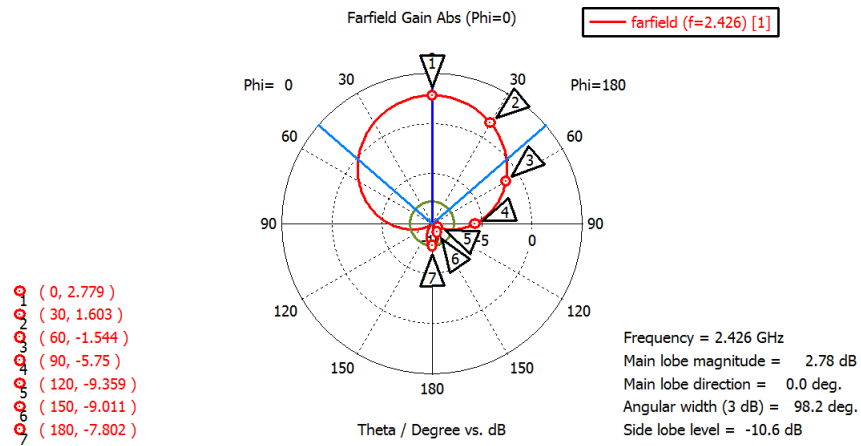


Figure 4.19: The gain of the SPA

Chapter 5

Evaluation Setup

There has been given a brief overview of the most important aspects regarding this project. In this section the different the tools for performing the simulations and real life scenario tests will be described.

5.1 CST Microwave Studio

The CST Microwave Studio is a computer aided program for the 3D electromagnetic simulation of high frequency components. It enables the analysis of high frequency devices such as antennas. The simulation setup can be briefly described in Figure 5.1.

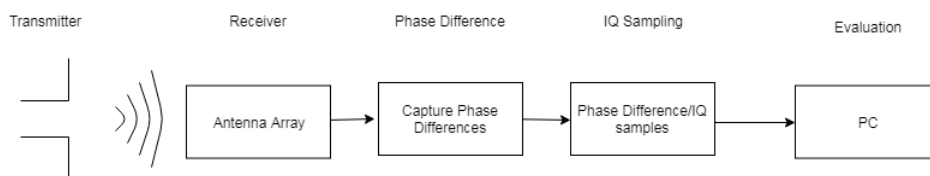


Figure 5.1: Simulation setup.

Firstly, the simulation provides the phases of the signal when it hits the receiver antennas. Then the phase difference is calculated. The phase differences are converted into IQ samples. The phase differences without discontinuities are now calculated using 2.13. Finally, the AoA is calculated using the phase differences.

5.2 Test setup

The test setup is attributed to Martin Englund [21]. The test setup can be briefly described in Figure 5.2.

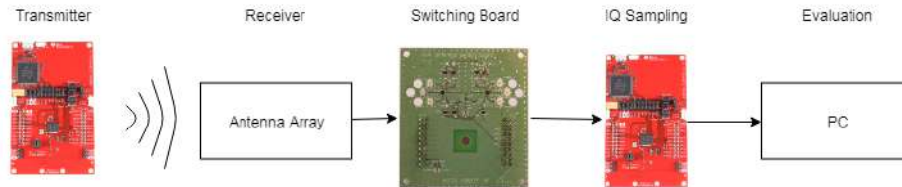


Figure 5.2: Test setup.

In short, the switching board chooses which antenna the launch pad will sample. After the IQ sampling of both antennas is done, the IQ samples are sent to the computer for evaluation and AoA estimation.

The tests were conducted with the use of a laptop, two CC2640R2 Development Kits by Texas Instruments, antennas, a switching board, photography equipment, a laser distance measure device and a protractor. The programs used to conduct the tests were MatLab and Code Composer Studio. The tests were conducted in two separate rooms in Assa Abloy Shared Technologies. The first room is the Radio Frequency Anaechoic Chamber and the second room is the Concept Lab which will be discussed in more detail in later sections. A setup can be seen in Figure 5.3. A simplified figure can be seen in 5.4.



(a) Angle 1.



(b) Angle 2.

Figure 5.3: One test setup from two different angles.

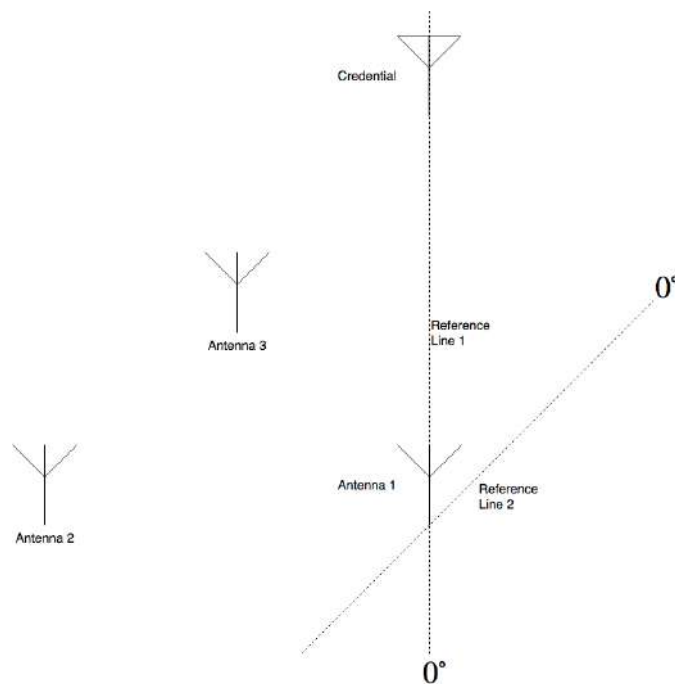


Figure 5.4: A simplified model of Figure 5.3.

In Figure 5.3a the transmitter and receiver are inside Radio Frequency Anaechoic Chamber (RFAC). The transmitter is on the left side while the receiver is on the right side. The receiver side is connected to a laptop outside of the RFAC. To estimate the angle of a credential, the transmitter is placed at a fixed distance. (Note: What is important is that the credential is at a distance in the farfield). The distance is approximately 0.6 meters away from the receiver.

The receiver in Figure 5.3 is comprised of three antennas. The reference line between two antennas is a hypothetical line that is perpendicular to the a hypothetical line that runs through the feeding points of the two antennas in question. Figure 5.4 shows the position of the credential, the receiving antennas and the reference lines that run through them from top view.

The standard test algorithm follows as:

1. Place the credential at -90° in reference to reference line 1.
2. Measure the angle of arrival.
3. Place the credential at $+30^\circ$ more than the previous angle.

4. Measure the angle of arrival.
5. Repeat until the credential is at $+90^\circ$ in reference to reference line 1.

The steps can change depending on the situation. For a better resolution more angles are needed. This can be solved by decreasing the angle step in step number three. In addition for an all around test, the credential must be placed from -179° to 180° . This can be done by changing steps one and five. Finally reference line two can be added in step one and step five to solve the problem discussed in 2.6.

If the measurements correlate to the real values of the angles, then the test can be conducted in more realistic environments. This environment in question is the Concept Lab at the Assa Abloy Shared Technologies office. In this room the same test will be performed for three different scenarios. The scenarios are Line-of-Sight, Wooden Door and Metal Door. These scenarios will be discussed in more detail in later sections.

5.3 Texas Instruments Evaluation Board

The equipment used for the test is the CC2640R2 Development Kit by Texas Instruments. It is a wireless microcontroller (MCU) targeting Bluetooth 4.2 and Bluetooth 5 low-energy applications [36]. For more information and details about the CC2640R2 you can refer to [21]. One of the CC2640R2 kits is used as the credential. This is done by implementing the 2.4-GHz Inverted F Antenna as a transmitting antenna [25]. The antenna can be seen in Figure 5.5. The antenna will be discussed in more detail in a later chapter.



(a) Front.

(b) Back

Figure 5.5: The CC2640R2 Development Kit.

5.4 Texas Instruments Antenna Credential

The antenna which is used as a credential is shown in the bottom side of Figure 5.5b. Figure 5.6 shows the 2.4-GHz Inverted F Antenna used in the CC2640R2 Development Kit. The dimensions can be viewed in Table 5.1

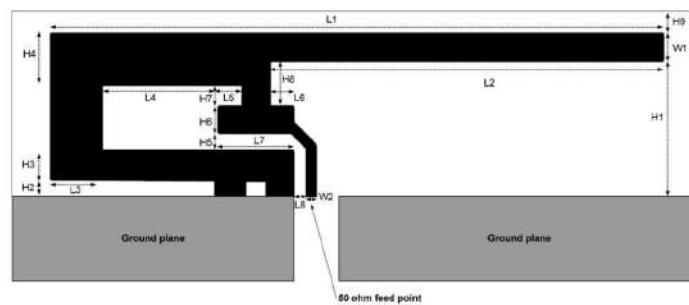


Figure 5.6: Texas Instruments 2.4-GHz Inverted F Antenna.

Parameter	Length	Parameter	Length
H1	5.70 mm	W2	0.46 mm
H2	0.74 mm	L1	25.58 mm
H3	1.29 mm	L2	16.40 mm
H4	2.21 mm	L3	2.18 mm
H5	0.66 mm	L4	4.80 mm
H6	1.21 mm	L5	1.00 mm
H7	0.80 mm	L6	1.00 mm
H8	1.80 mm	L7	3.20 mm
H9	0.61 mm	L8	0.45 mm
W1	1.21 mm		

Table 5.1: IFA Dimensions

This antenna falls under the Inverted F antennas (IFA) category.

The IFA is very similar to a wire antenna, however due to the reason why the antenna radiates it resembles more an aperture antenna. Specifically the feed is placed from the ground plane to the upper arm of the IFA. The length of the arm is approximately a quarter of a wavelength. The polarization is vertical and the ground plane has a length and width of approximately the length of the arm. It is important to note that the width must be at least a quarter of a wavelength long. A smaller height decreases the bandwidth and the efficiency of the antenna. The distance between the ground plane and the upper arm of the IFA should be a fraction of a wavelength. However the height does not drastically change the impedance and radiation properties.

In order to understand why the IFA radiates, the slot antenna must be discussed first. A slot antenna is one of the simplest antennas that can be made. They have an omnidirectional radiation pattern and the different slot sizes and shapes can offer a variety of potential parameters to tune.

When the slot of the antenna is induced with electromagnetic fields the slot structure becomes an antenna. When the slot is induced with electromagnetic fields an electric field is distributed within the slot while the currents travel around the slot. The dual of a slot antenna would be created if the conductive material and air were interchanged. Babinet's principle relates the slot antennas to its dual [37]. However

the dual resembles a dipole antenna. Figure 5.7 depicts the principle. The two antennas are the same expect from the fact that the fields are interchanged. In other words a slot antenna is simply a dipole antenna turned by 90° .

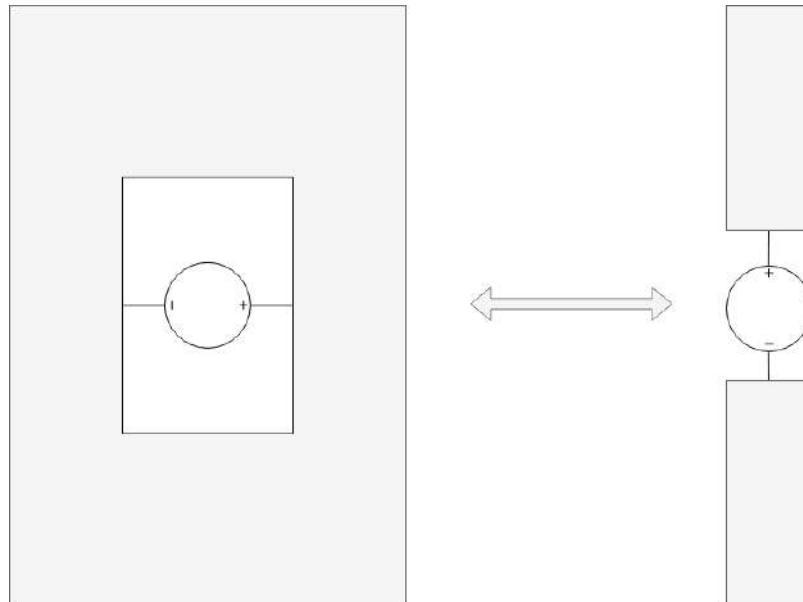


Figure 5.7: The slot antenna and the dipole antenna.

The slot antenna is short circuited at the edges of the slot which implies that the voltage will be minimum. If the antenna is viewed as a transmission line it would mean that the voltage and current are 90° out of phase. This means that the current at the center of the slot antenna is zero whereas it is maximum at the edges.

This is very important because if the the current is zero at the center of the slot it means that it is an open circuit at the center. By cutting the slot in half the antenna has zero current and maximum voltage at that place. This is the same case as with the slot antenna. The slot antenna is practically a half a slot antenna which is an IFA.

IFA antennas are widely used in mobile phones. The reason for this is the small size which is around a quarter of a wavelength in length. When implemented with a dielectric between the upper arm and the ground plane the size can be reduced even further. However this will decrease the efficiency drastically.

The following specifications are given from Texas Instruments 2.4 Inverted F Antenna in [25]. The antenna size is $25.7 \times 7.5 \text{ mm}$. Figure 5.8

provides the bandwidth of the antenna. The antenna ensures a 10% reflection for the available power for a bandwidth of more than 300 MHz. This means that it requires no tuning that would otherwise mismatch the antenna due to the objects in the close vicinity [25]. Table 5.2 provides the summary of the highest gain in with different orientations of the antenna.

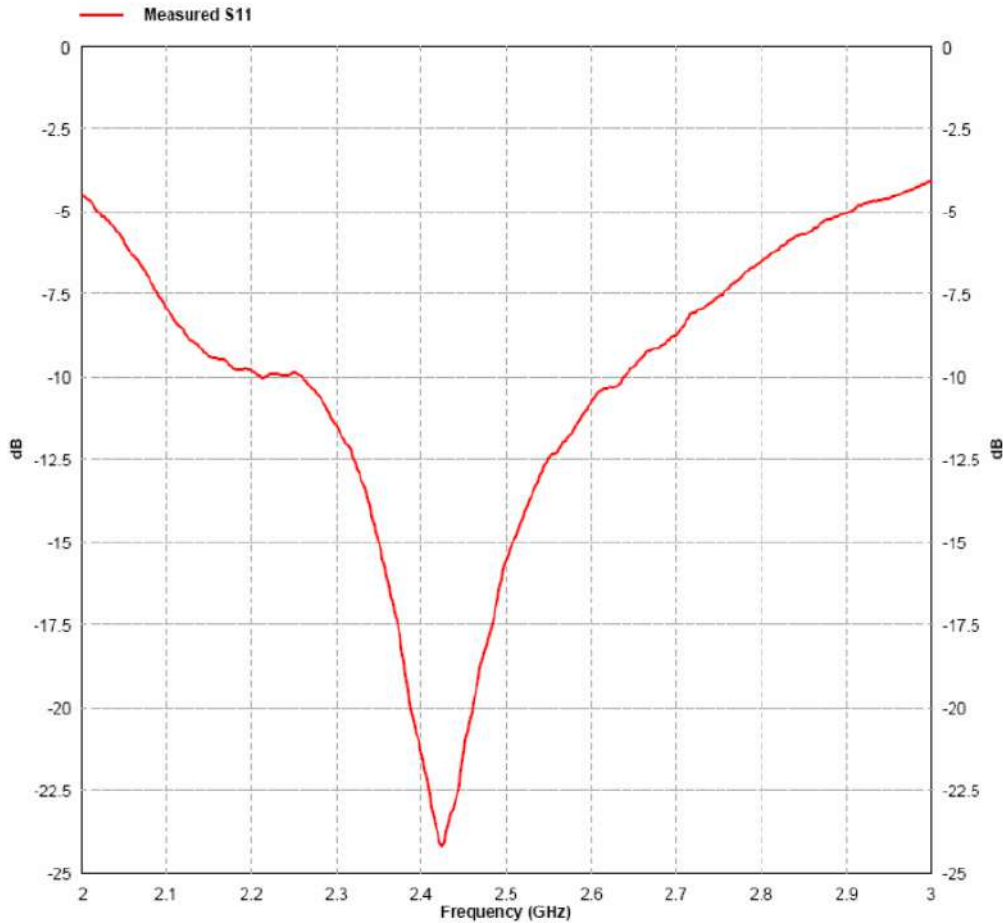


Figure 5.8: Measured reflection at the feed point of the antenna.

5.5 Radio Frequency Anechoic Chamber

ASSA ABLOY Shared Technologies has a radio frequency anechoic chamber or commonly known an EMC chamber. The word anechoic

Plane	Gain
XY	1.1 dBi
XZ	3.3 dBi
YZ	1.6 dBi

Table 5.2: Gain in different orientations for the TI IFA.

means without echo. The key characteristics of these chambers is that they absorb all reflected waves within the chamber. This means that there will be no reflections from the walls, floor and ceiling. In addition, they provide shielding from outside unwanted interference.

5.6 Line of Sight

The line of sight test was conducted in the Concept Lab at the ASSA ABLOY Shared Technologies office. The test was conducted in the middle of the laboratory without considering laptops, mobile phones and other electronic equipment that were present at the time. The tests were inconclusive and were not included in this thesis.

5.7 Wooden Door

The wooden door test was conducted in the Concept Lab at the ASSA ABLOY Shared Technologies office. It is a similar test to the line of site test in section 5.6. In this test the receiver antenna design was placed on a wooden door close to the handle. The tests were inconclusive and were not included in this thesis.

5.8 Metal Door

The metal door test was designed in the Concept Lab at the ASSA ABLOY Shared Technologies office. It is a similar test to the line of site test in section 5.7. Due to time and results constraints the test was not conducted.

Chapter 6

Results and Discussion

The presentation of the final results will be in this chapter. Firstly, the expected results are going to be shown in Figure 6.1. The x-axis show the true angle that the credential is placed while the y-axis shows the measured angle.

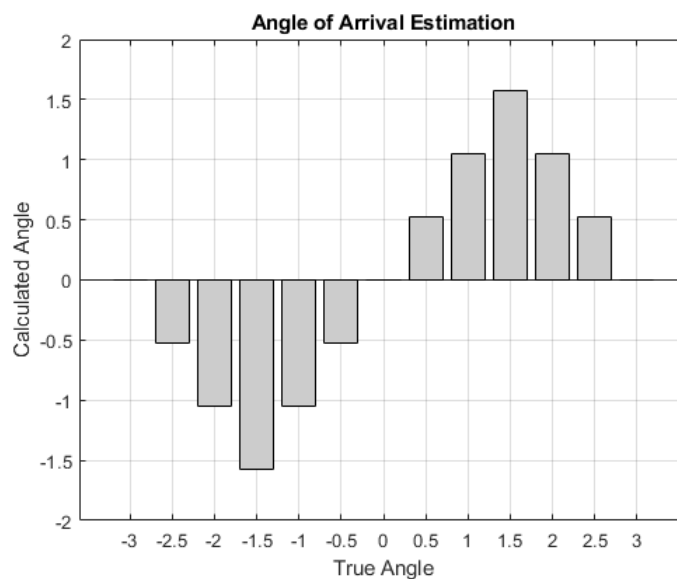


Figure 6.1: Angle of Arrival theoretical results.

A test was conducted using using delaylines. For more information about this test refer to [21]. Figure 6.2 depicts the results from these delaylines. The bar shows the mean while the black shows the standard deviation of the results.

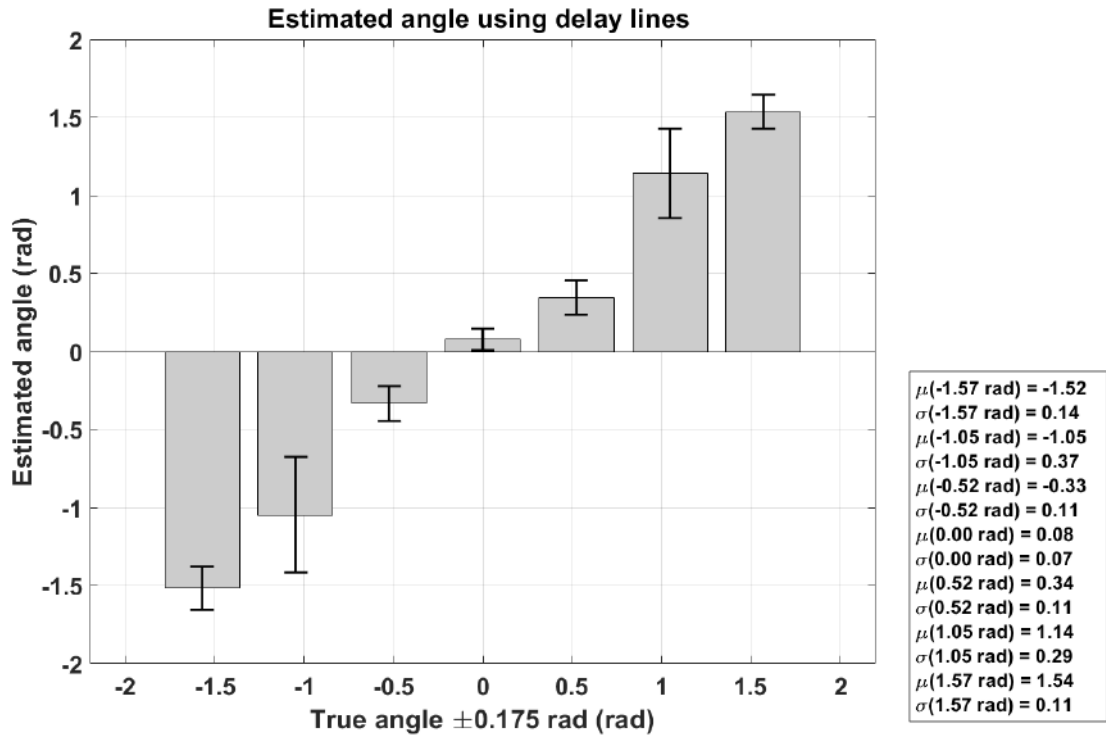


Figure 6.2: Angle of Arrival Estimation using delaylines.

The figure is quite interesting. It shows that even with the delay-lines the results are not perfect. In addition, [21] argues that the error exponentially increases in the $\pm 60^\circ$ region. This is confirmed in the figure. The aforementioned region has the highest sigma, meaning that the result variations in this region are the highest.

The antennas designed were simulated and the phase difference was calculated. This was achieved by checking the difference phases that each antenna has for the different angles at which a transmitter was placed. The transmitter was a discrete port which was simulating a dipole antenna operating at 2.426 GHz. After that, the IQ samples were calculated with the following equations where I_1, Q_1, I_2, Q_2 and P_1, P_2 are the IQ samples and phases of the antennas in question respectively.

$$I_1 = \cos(P_1) \quad (6.1)$$

$$Q_1 = \sin(P_1) \quad (6.2)$$

$$I_2 = \cos(P_2) \quad (6.3)$$

$$Q_2 = \sin(P_2) \quad (6.4)$$

After that, the algorithm based on [21] was used to fix discontinuities. This was done in two steps. Firstly, the phase difference is calculated using the following equation, where P_d is the phase difference:

$$P_d = \arctan2((I_1 + Q_1i) * (I_2 + (-1 * Q_2)i)) \quad (6.5)$$

Then, the angle must be calculated using the phase difference and the distance between the receiver as discussed in Section 2.6 using the following equation, where α is the angle at which the transmitter is placed, λ is the wavelength of the electromagnetic wave and d is the distance between the two antenna elements that act as a receiver:

$$\alpha = \text{Real}\left(\frac{P_d * \lambda}{2\pi} / d\right) \quad (6.6)$$

The results from the simulations are going to be shown in three steps. In the first step, the phase differences from the receiver will be shown. In the second step, the phase difference calculation from the IQ sampling will be shown. In the third step, the Angle of Arrival will be calculated from the phase differences. The final Angle of Arrival results from the real life experiment will be shown. The results will be shown in radians.

Finally, it is important to show Figure 6.3.

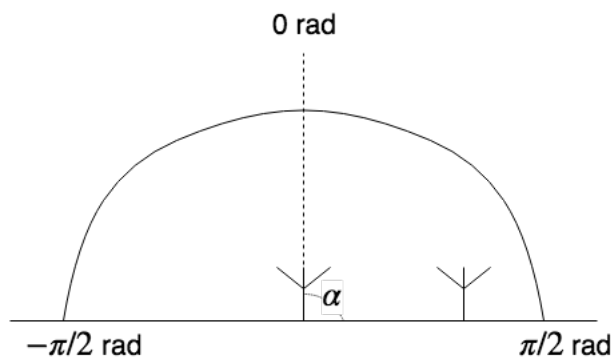


Figure 6.3: Reference line and angle measurement in comparison to the antenna placement

It is important to know that the reference line is perpendicular to the line that passes through two antennas that the AoA is measured.

6.1 First Iteration

The tests were conducted in two iterations. The first iteration involved five different antenna elements that were made using printed circuit board technology. The antennas were printed on a 0.4 mm FR-4 laminate.

6.1.1 Square Ring Antenna

In this section the results from the square ring patch antennas will be presented. In Figure 6.4 one can see how the antennas are placed. The credential was placed at 0.7m centimeters away from the antennas and was circled around the receiver antennas from -180° to 180° with a 10° increment in each step in the simulation and from -150° to 180° with a 30° increment in each step in the experiment. The distance between the receiver antennas is 30.9mm.

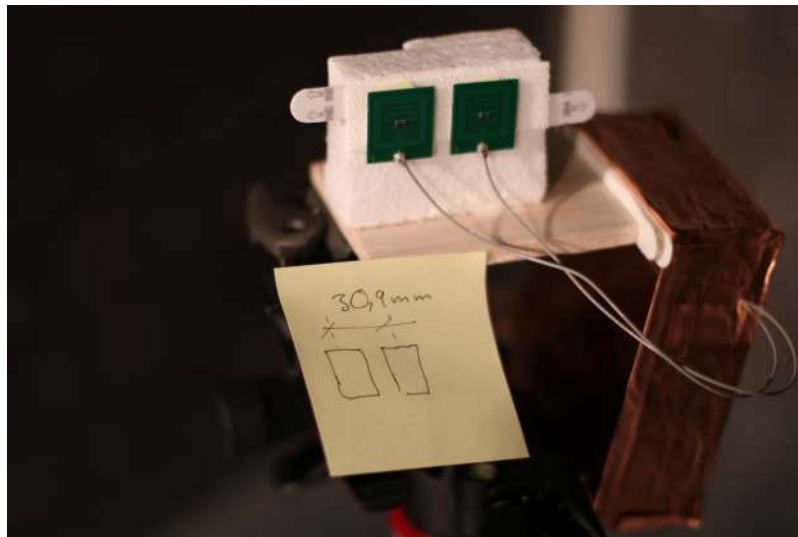


Figure 6.4: The two square ring meandered antennas on test site.

The test setup was simulated and the results can be seen in Figures 6.5. The Figure shows the relative phase difference between the antennas for different angles that the credential was placed.

Firstly, the phase differences from the receiver will be shown. Figure 6.5 shows the simulated phase differences.

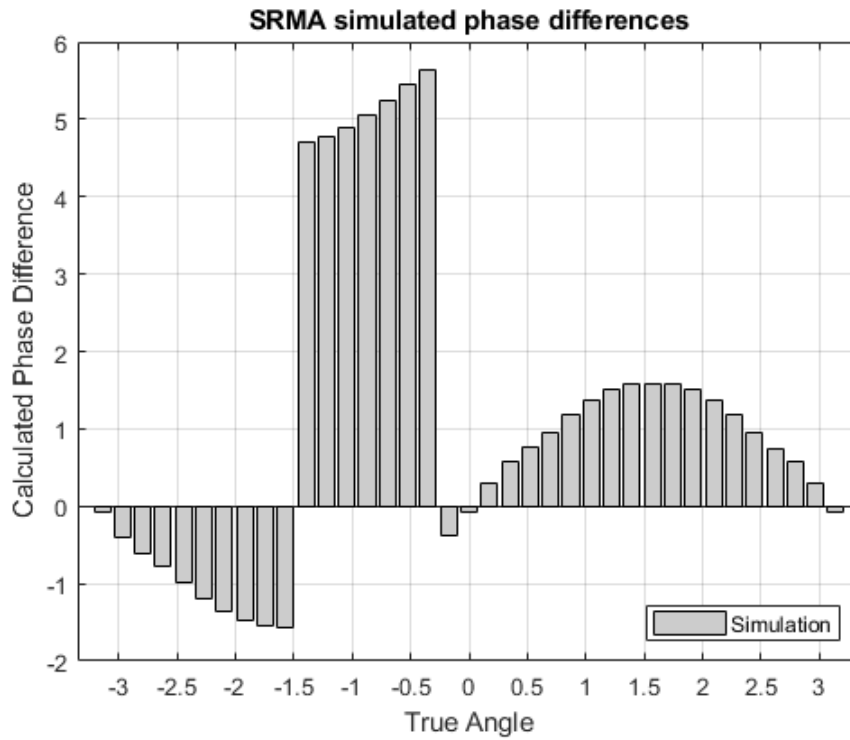


Figure 6.5: Simulated phase differences between the two square ring meandered antennas.

After that the IQ samples were calculated using the equations 6.6, 6.2, 6.3 and 6.4. Using the IQ samples and the equation 6.5, the resulting phase differences can be seen in Figure 6.6.

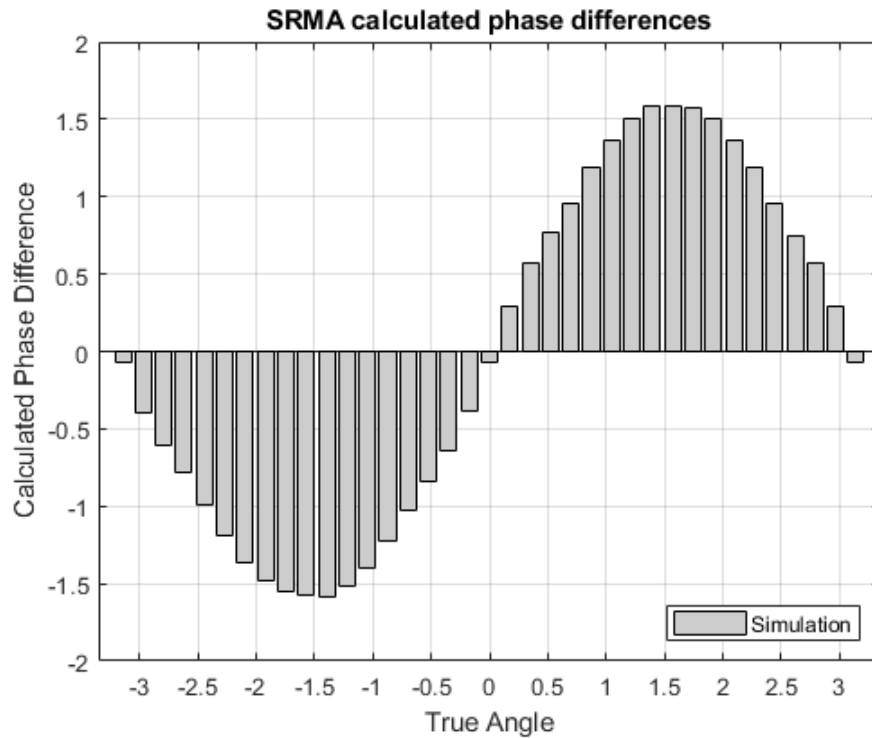


Figure 6.6: Calculated phase differences between the two square ring meandered antennas.

The results show that the algorithm is compensating for the angle drift. The reason for this is that the relative phase difference does not take into consideration the speed of the electromagnetic wave and the distance between the antennas. In this case the speed is the same as the speed of the electromagnetic wave operating at channel 38 and the distance between the antennas is $31mm$. Using Equation 6.5 the Angle of Arrival can be calculated. Figure 6.7 shows the Angle of Arrival estimation from the provided phase differences.

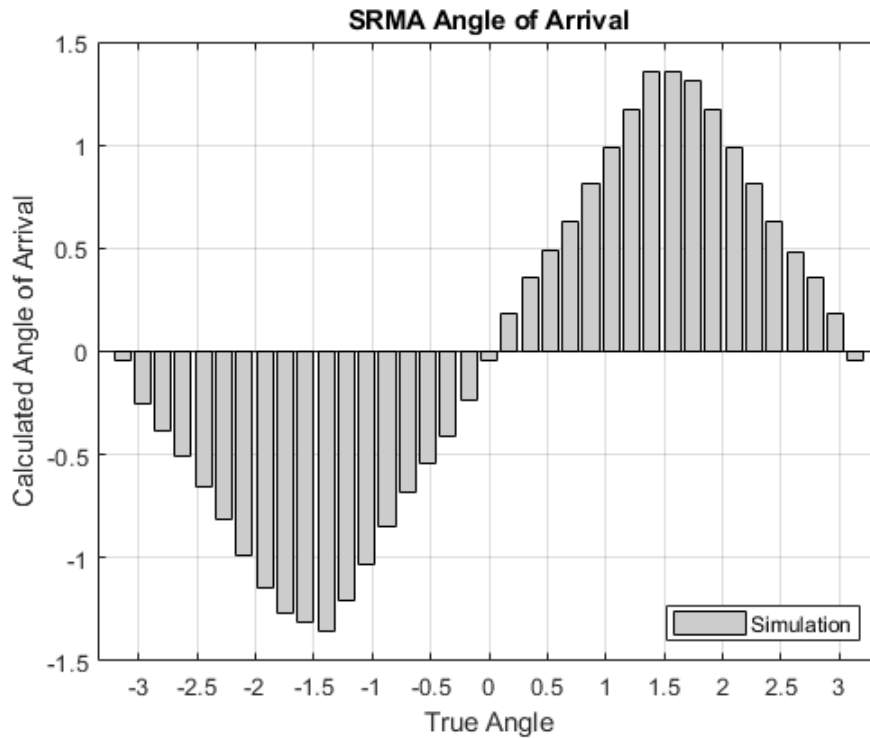


Figure 6.7: Calculated Angle of Arrival between the two square ring meandered antennas.

The results show extreme resemblance to the theory. The calculated Angle of Arrival follow the theoretical true angles. The minor differences are attributed to the fact that the reference line must cross through the middle of antenna 1. Therefore, the EM will take more time to reach antenna 2 which results in a small difference in values.

The same test setup was used in an experiment in the EMC chamber. The credential was placed at a horizontal polarization at a distance of $0.7m$. The results can be seen in Figure 6.8.



Figure 6.8: Angle of Arrival Estimation using the square ring meandered antennas.

The results show no similarities with the theory. The low gain of the antenna could render the receiving signal low enough for noise to play a bigger role in determining the angle.

6.1.2 NPA

In this section the results from the normal patch antennas will be presented. In Figure 6.10 one can see how the antennas are placed. The credential was placed at $0.7m$ centimeters away from the antennas and was circled around the receiver antennas from -180° to 180° with a 10° increment in each step in the simulation and from -90° to 90° with a 30° increment in each step in the experiment. The distance between the receiver antennas is $32mm$.

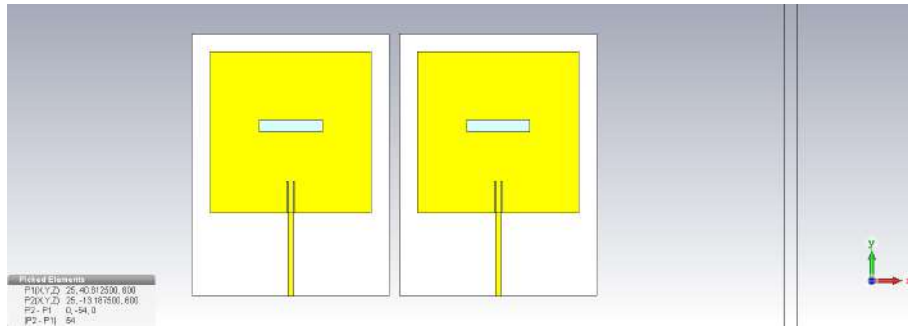


Figure 6.9: Test setup of the normal patch antennas.

The test setup was simulated and the results can be seen in Figures 6.10. The Figure shows the relative phase difference between the antennas for different angles that the credential was placed.

Firstly, the phase differences from the receiver will be shown. Figure 6.10 shows the simulated phase differences.

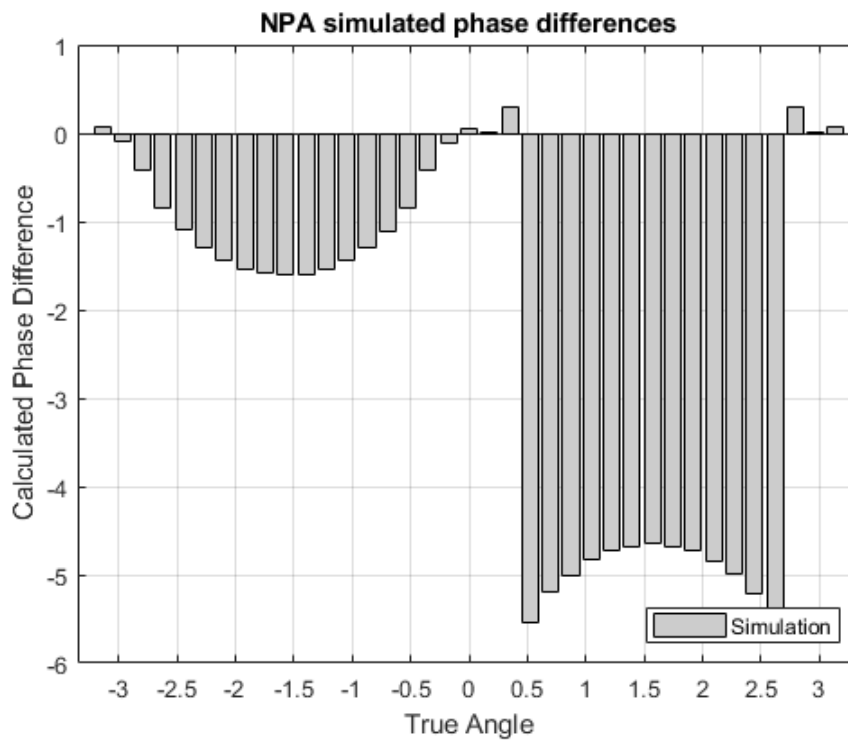


Figure 6.10: Simulated phase differences between the two normal patch antennas.

After that the IQ samples were calculated using the equations 6.6,

6.2, 6.3 and 6.4. Using the IQ samples and the equation 6.5, the resulting phase differences can be seen in Figure 6.11.

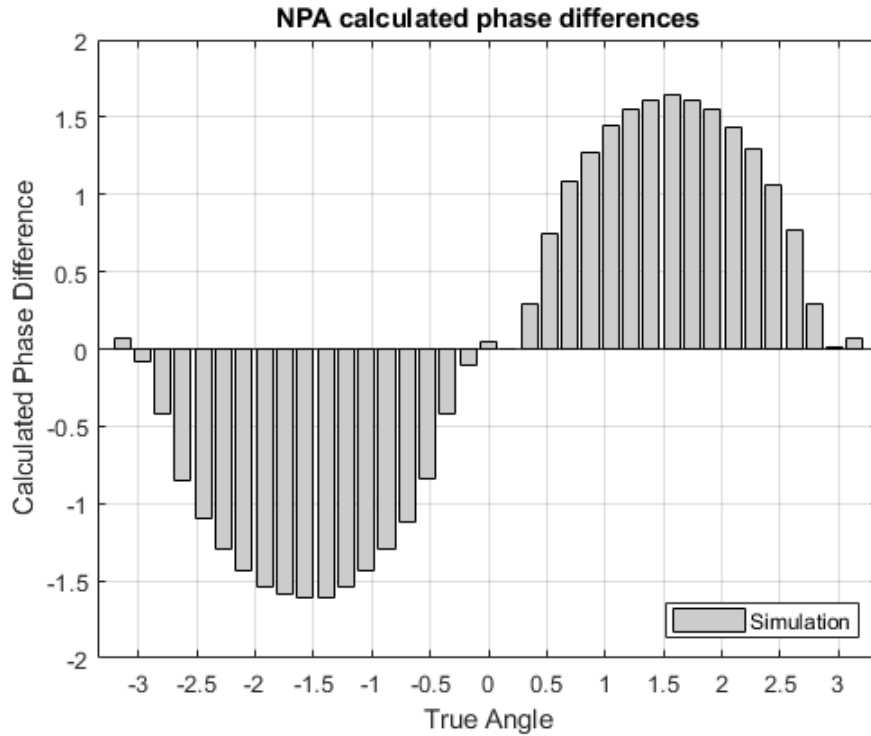


Figure 6.11: Calculated phase differences between the two normal patch antennas.

The results show that the algorithm is compensating for the angle drift. The reason for this is that the relative phase difference does not take into consideration the speed of the electromagnetic wave and the distance between the antennas. In this case the speed is the same as the speed of the electromagnetic wave operating at channel 38 and the distance between the antennas is 31mm . Using Equation 6.5 the Angle of Arrival can be calculated. Figure 6.12 shows the Angle of Arrival estimation from the provided phase differences.

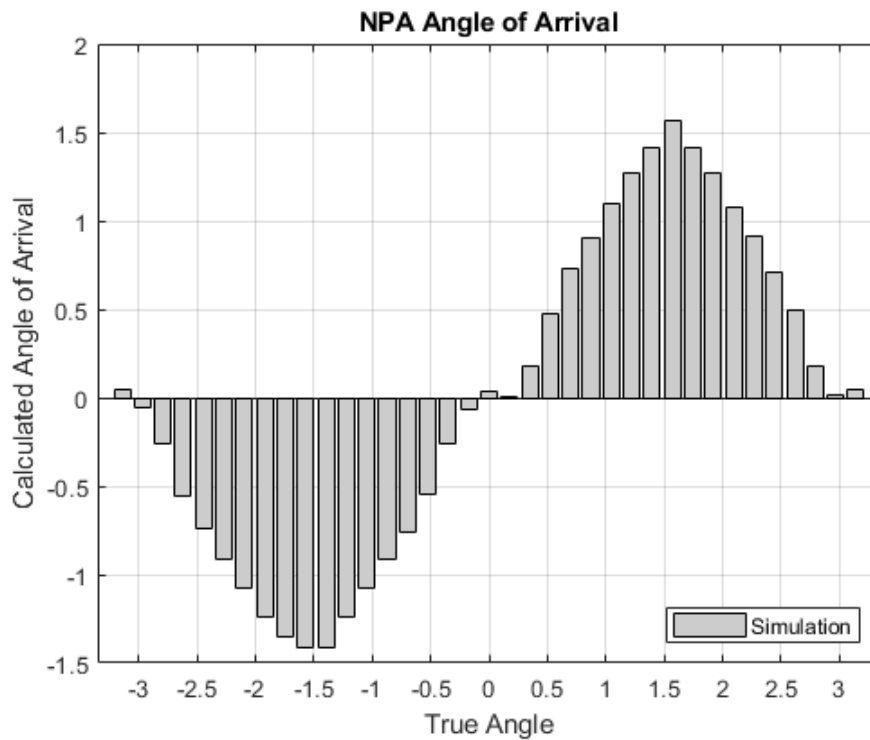


Figure 6.12: Calculated Angle of Arrival between the two normal patch antennas.

The results show extreme resemblance to the theory. The calculated Angle of Arrival follow the theoretical true angles.

The same test setup was used in an experiment in the EMC chamber. The credential was placed at a horizontal polarization at a distance of $0.7m$. The results can be seen in Figure 6.13.

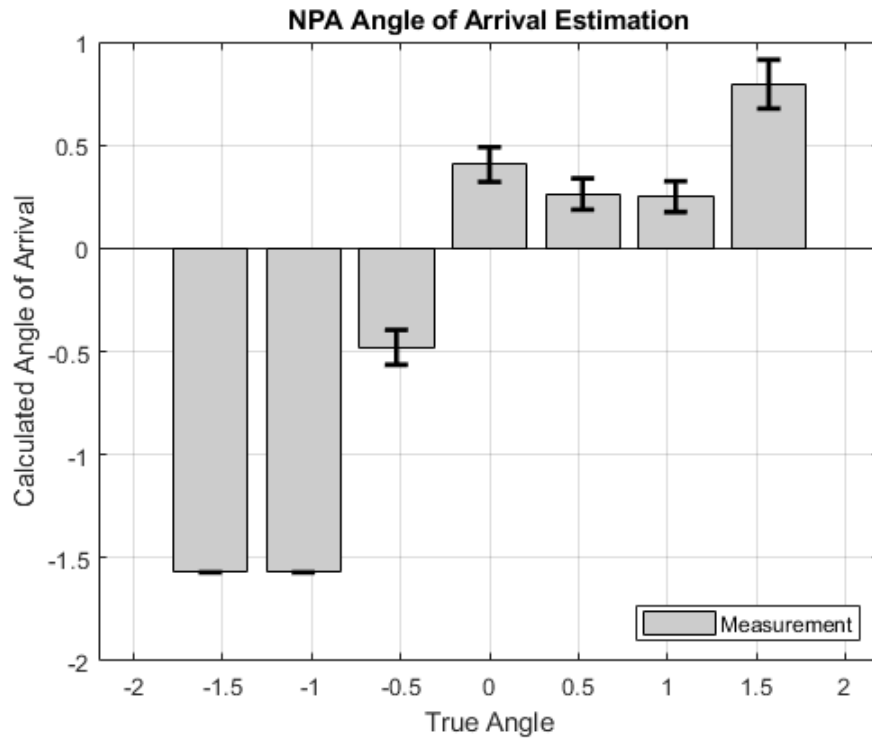


Figure 6.13: Angle of Arrival Estimation using the normal patch antennas.

The results show no similarities with the theory. The low gain of the antenna could render the receiving signal low enough for noise to play a bigger role in determining the angle.

6.1.3 Circularly Polarized Patch Antenna

In this section the results from the normal patch antennas will be presented. In Figure 6.14 one can see how the antennas are placed. The credential was placed at $0.7m$ centimeters away from the antennas and was circled around the receiver antennas from -180° to 180° with a 10° increment in each step in the simulation and from -90° to 90° with a 30° increment in each step in the experiment. The distance between the receiver antennas is $32mm$.

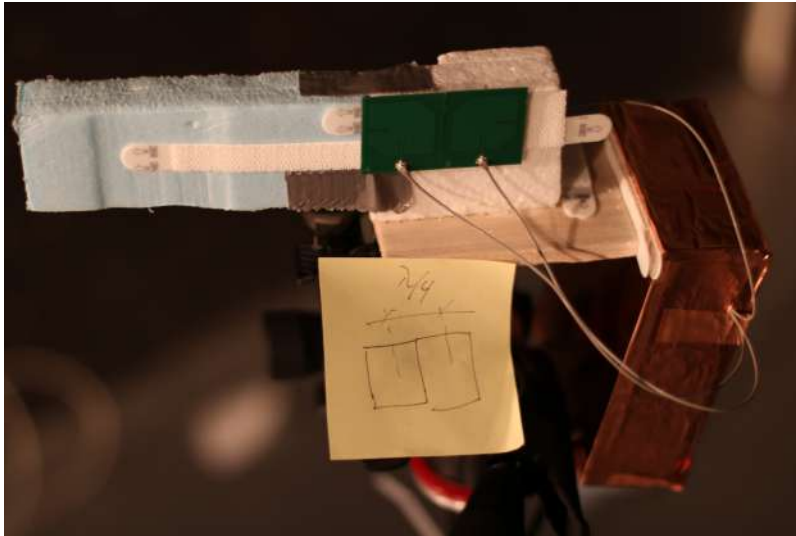


Figure 6.14: Angle of Arrival Estimation using the circularly polarized patch antennas.

The test setup was simulated and the results can be seen in Figures 6.14. The Figure shows the relative phase difference between the antennas for different angles that the credential was placed.

Firstly, the phase differences from the receiver will be shown. Figure 6.15 shows the simulated phase differences.

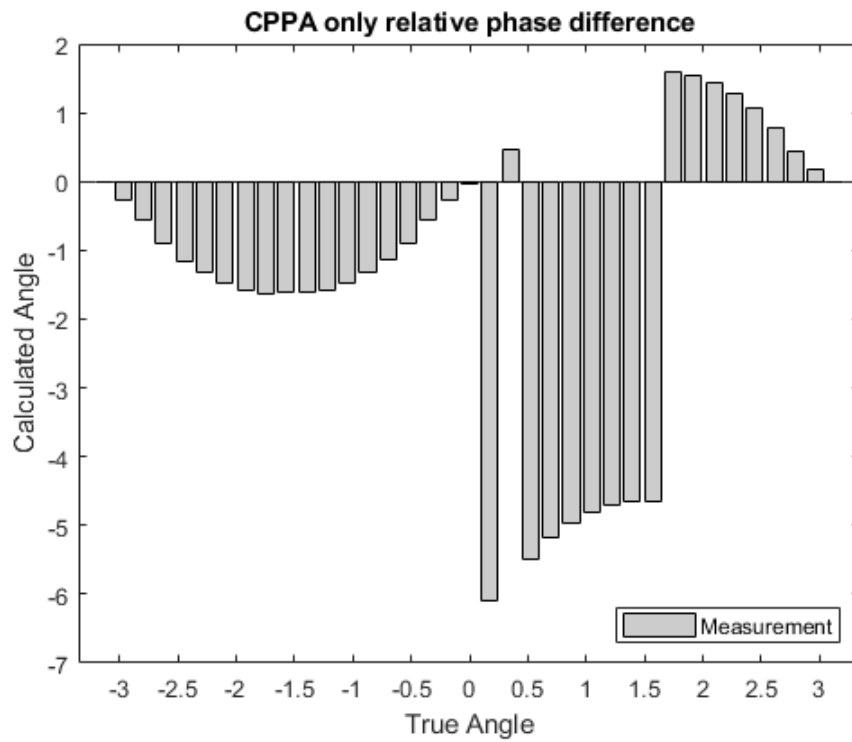


Figure 6.15: Simulated phase differences between the two circularly polarized patch antennas.

After that the IQ samples were calculated using the equations 6.6, 6.2, 6.3 and 6.4. Using the IQ samples and the equation 6.5, the resulting phase differences can be seen in Figure 6.16.

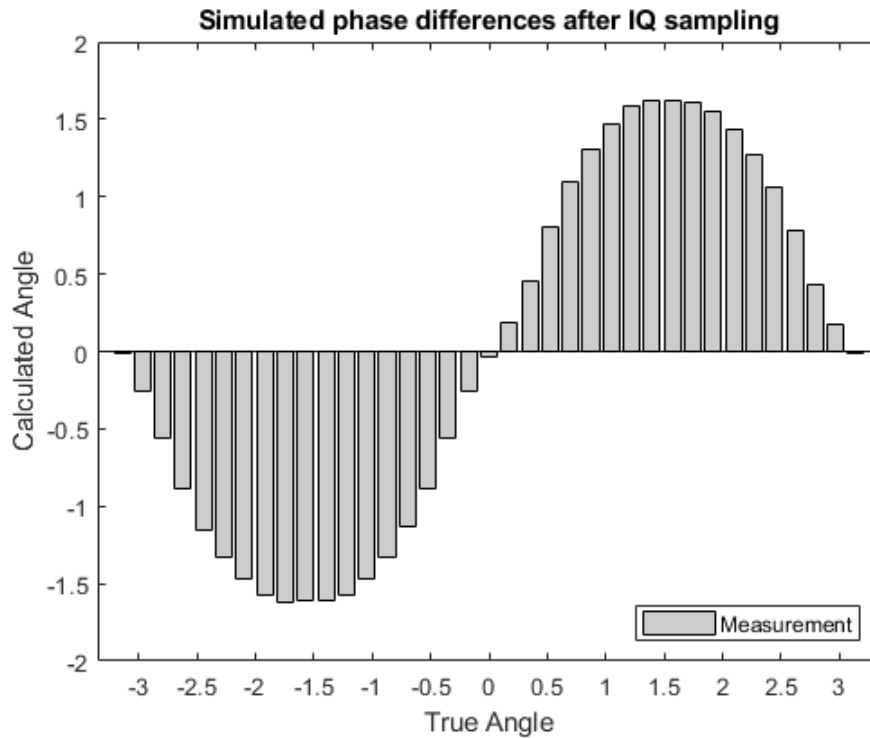


Figure 6.16: Calculated phase differences between the two circularly polarized patch antennas.

The results show that the algorithm is compensating for the angle drift. The reason for this is that the relative phase difference does not take into consideration the speed of the electromagnetic wave and the distance between the antennas. In this case the speed is the same as the speed of the electromagnetic wave operating at channel 38 and the distance between the antennas is $31mm$. Using Equation 6.5 the Angle of Arrival can be calculated. Figure 6.17 shows the Angle of Arrival estimation from the provided phase differences.

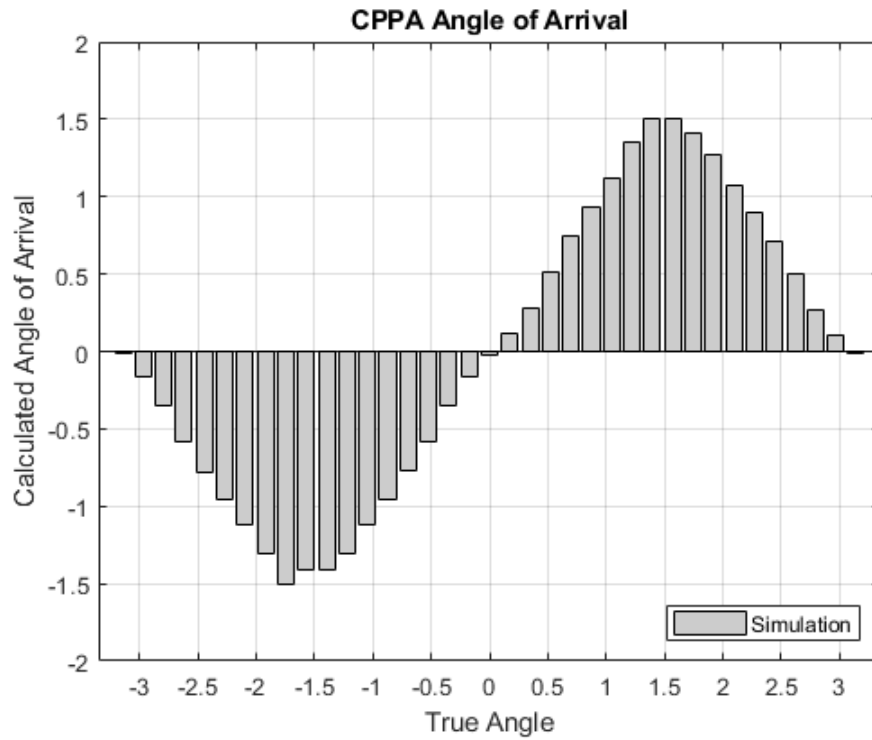


Figure 6.17: Calculated Angle of Arrival between the two circularly polarized antennas.

The results show extreme resemblance to the theory. The calculated Angle of Arrival follow the theoretical true angles.

The same test setup was used in an experiment in the EMC chamber. The credential was placed at a horizontal polarization at a distance of $0.7m$. The results can be seen in Figure 6.18.

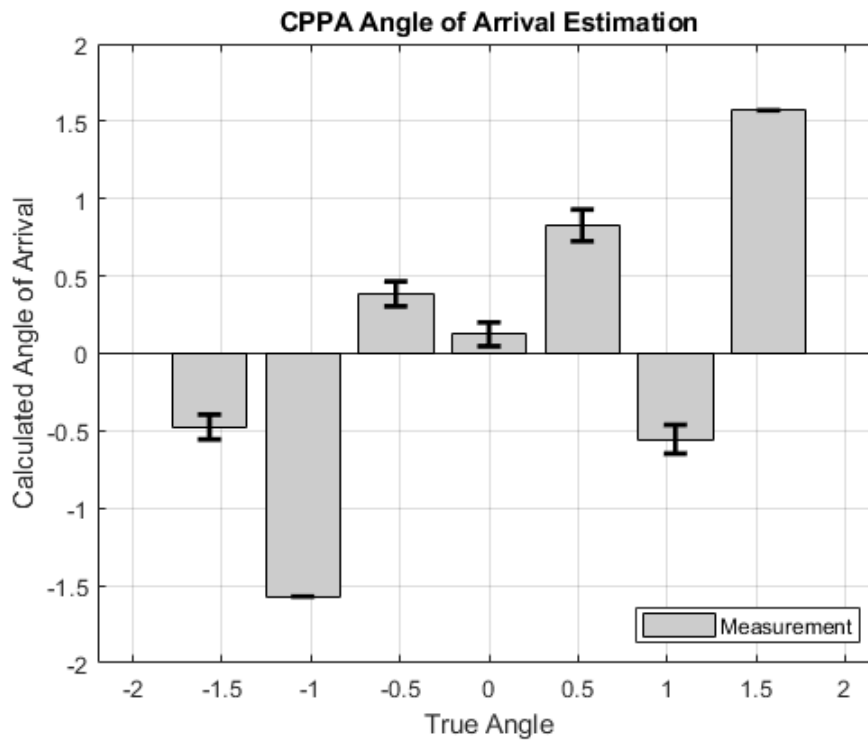


Figure 6.18: Angle of Arrival Estimation using the circularly polarized patch antennas.

The results show no similarities with the theory. The low gain of the antenna could render the receiving signal low enough for noise to play a bigger role in determining the angle.

6.1.4 Summary

Clearly the results from the simulations and the experiments differ a lot. There are three main differences between the simulations and the experiments. Firstly, the receiver in the experiment uses cables, connectors and two PCBs that are potentially decreasing the strength of the receiving signal due to mismatches. Secondly, the antenna used as a credential is different in the two cases. In the first case, the credential is a perfect dipole while in the second case, it is an IFA antenna whose properties are not known to a full extent. Finally, the implementation of the system does not match the proposal. Specifically the system is not suitable for use in a product [21].

6.2 Second Iteration

The first iteration provided unsatisfactory results. The antenna elements with the worst results had in common an extremely low gain, unsatisfactory axial ratio, narrow beamwidth and were circularly polarized except from the NPA. The NPA antennas did not provide satisfactory results but the monotonous increase in the resulting angles showed that the increased gain and correct polarization impact the AoA estimation the most in the experiments.

Therefore, in the second iteration the gain of the antenna elements was given more importance during the design process. In addition the antenna elements were designed to be linearly polarized in order to reduce the effect of polarization losses and in turn reduce potential power reduction. Moreover the antenna elements and the connectors were constructed by hand.

6.2.1 SPA

The handmade antenna elements are standard patch antennas (SPA) fed with a coaxial cable. The parameters of this antenna can be seen in Section 4.4.

Test One

In this section the results from the normal patch antennas will be presented. In Figure Figures 6.19 and 6.20 one can see how the antennas are placed. The credential was placed at $0.7m$ centimeters away from the antennas and was circled around the receiver antennas from -180° to 180° with a 10° increment in each step in the simulation and from -165° to 180° with a 15° increment in each step in the experiment. The distance between the receiver antennas is $51mm$.



Figure 6.19: Test setup of SPA antennas.

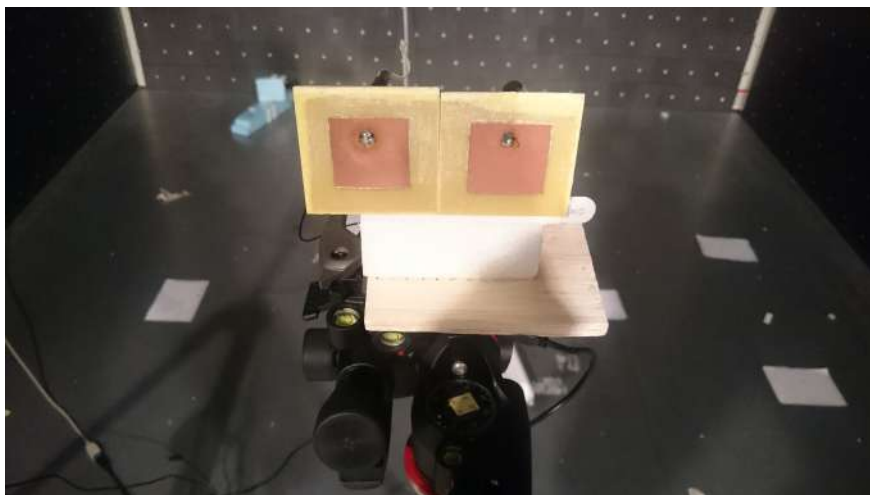


Figure 6.20: Closeup of test setup of the SPA antennas.

The test setup was simulated and the results can be seen in Figures 6.14. The Figure shows the relative phase difference between the antennas for different angles that the credential was placed.

Firstly, the phase differences from the receiver will be shown. Figure 6.21 shows the simulated phase differences.

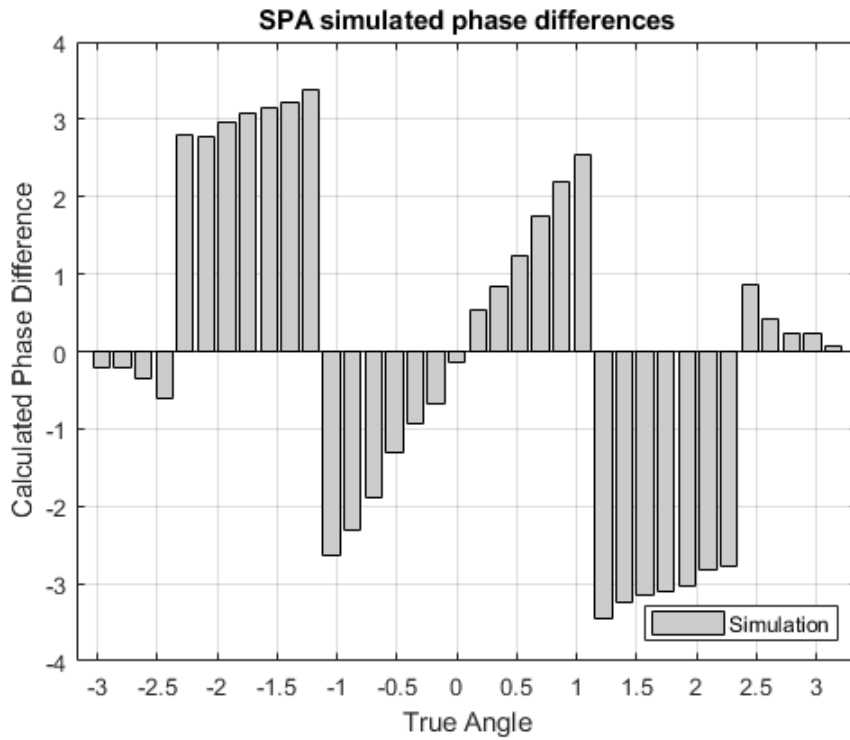


Figure 6.21: Simulated phase differences between the two standard patch antennas.

It is interesting to see that the relative phase difference is flipping two times in the case of the SPA antennas. After that the IQ samples were calculated using the equations 6.6, 6.2, 6.3 and 6.4. Using the IQ samples and the equation 6.5, the resulting phase differences can be seen in Figure 6.22.

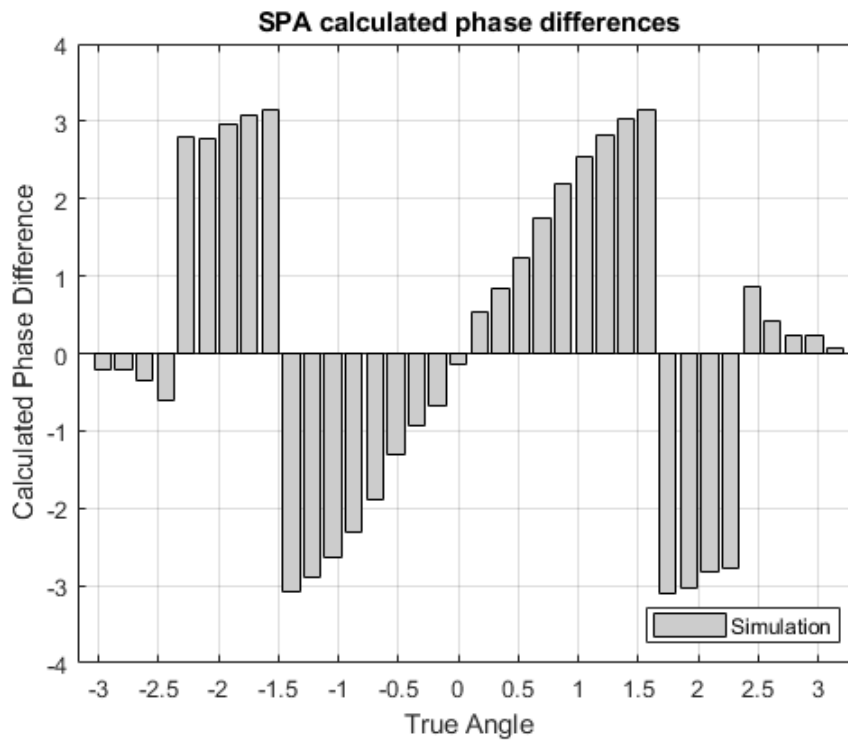


Figure 6.22: Calculated phase differences between the two standard patch antennas.

The results show that the algorithm is compensating for some angles while others are stayed unchanged. In this case the speed is the same as the speed of the electromagnetic wave operating at channel 38 and the distance between the antennas is 52mm. The next step is to normalize the angles according to the wavelength operating and the distance between the receiver antennas. Figure 6.23 shows the results.

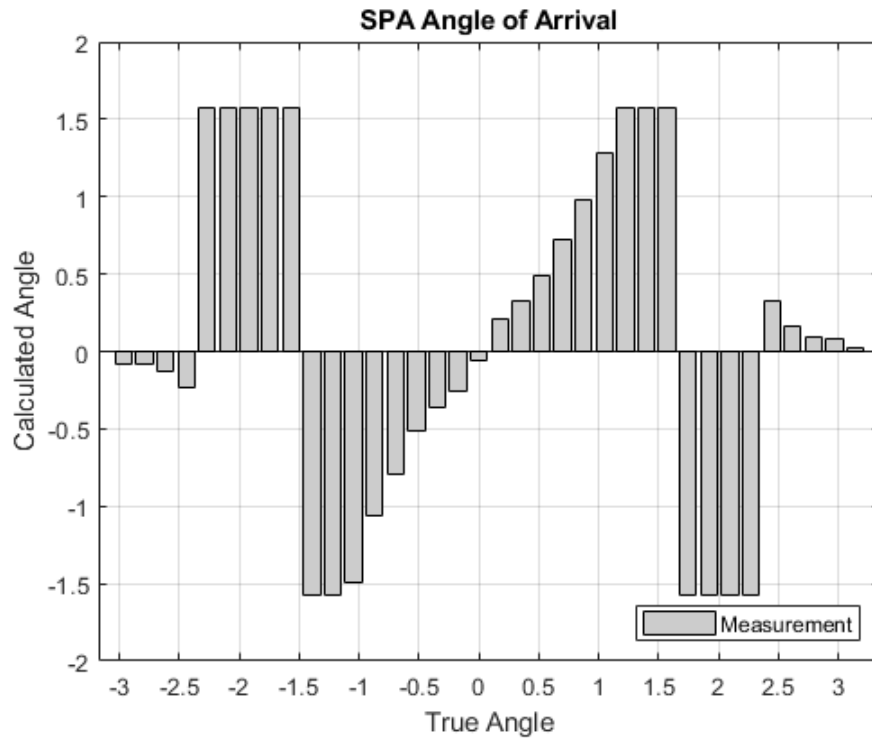


Figure 6.23: Angle of Arrival Estimation using the circularly polarized patch antennas.

The results do not correlate with the theory. The angles that are not compensated for are a potential problem. It is important to see why this happens. Figure 6.24 shows the results if the compensation algorithm was correctly compensating for all angles. The new compensation algorithm works in the following way. If the measured phase difference is outside of -155° and 155° , the angle is mirrored on the x-axis. This is done before the IQ samples were calculated.

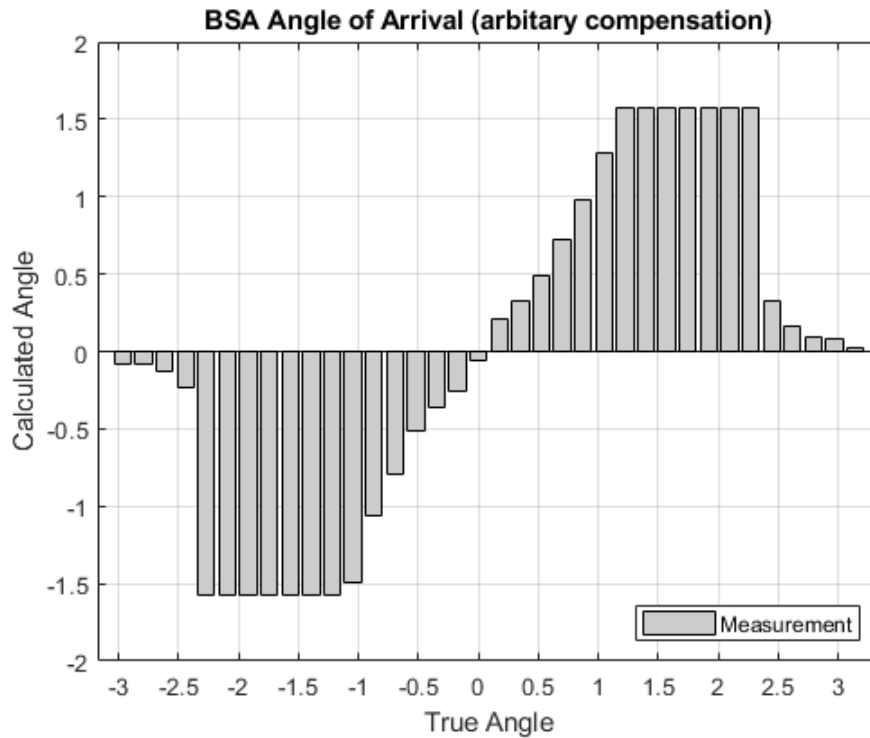


Figure 6.24: Angle of arrival estimation using the BSA antennas with arbitrary compensation.

The results show that before the -90° region and after the 90° region the angles are still increasing. This might be the reason the algorithm is not working for the IQ samples. The phase differences do not follow the pattern that is expected and therefore the algorithm does not compensate for those angles. Figure 6.25 show the final calculated Angle of Arrival.

The reason for this is attributed to the phase center. The incoming electromagnetic wave is approaching the antennas from two sides. While the credential is in the front of the feeding points of the antennas, the phase from both sides is the same. However, when the credential is placed behind the antennas, the electromagnetic wave will reach the feeding point but at a different time.

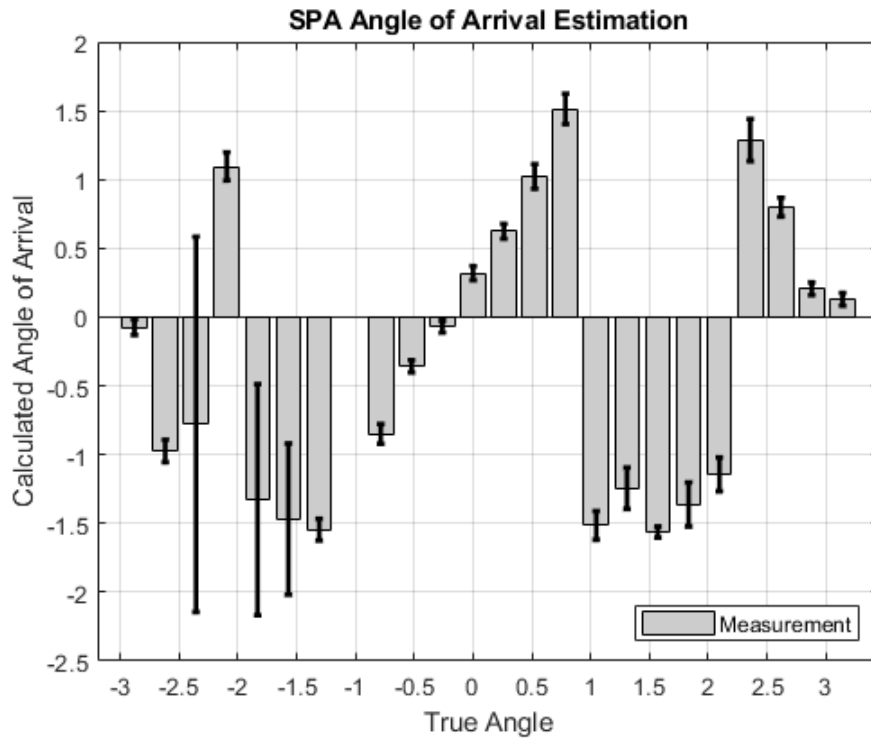


Figure 6.25: Angle of Arrival Estimation of BSA antennas.

The results are really interesting. There are two problematic regions. The first region is between angles -135° and -90° . Here the variance is high as seen from the long sigma. In addition the -120° is flipped and does not show the same sigma. The second region is between angles 60° and 120° there is a flipping to negative angles which we will call flip effect.

However, this correlates with the simulations. If the IQ compensation algorithm is not used there is a clear resemblance between the simulation and the experiment. Figure 6.26 shows this. In this simulation the IQ compensation algorithm was not used and the Angle of Arrival was directly calculated from the phase differences.

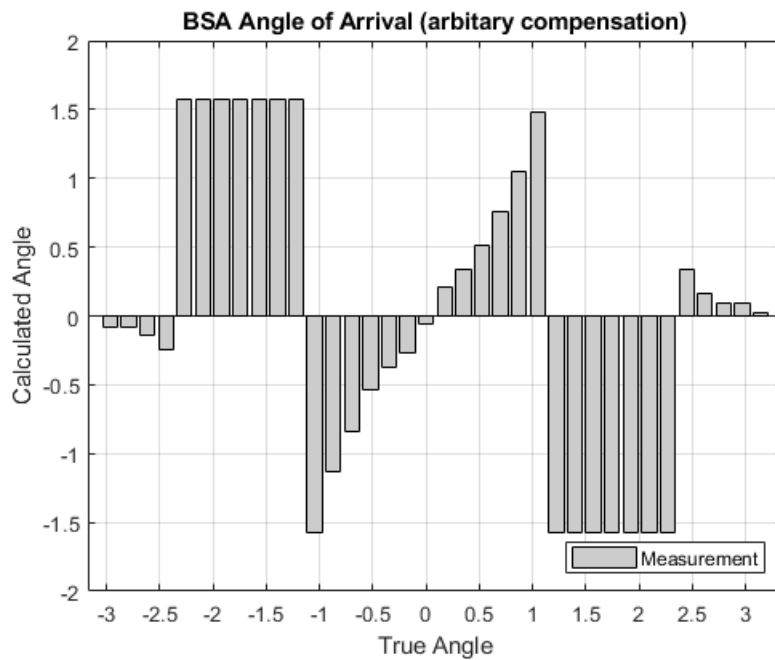


Figure 6.26: Angle of Arrival Estimation without IQ compensation.

In this Figure there is a clear indication as to what happens when the IQ compensation algorithm is not present. However, in the experiment the algorithm is present but is not working for all angles. If the IQ compensation algorithm was working as intended, then Figure 6.24 would be the same as the experiment result.

Therefore, there are three things that must be stated. Firstly, by significantly increasing the gain of the receiving antennas, the experiment and the simulations results are correlating. Secondly, the phase differences do not follow the triangular pattern that the other antennas follow in the previous simulations. There is a slight increase before -90° and after 90° and then there is an exponential decrease in phase differences. Finally the IQ compensation algorithm is not working as intended in this case.

Test Two

Since the problem arises when the credential is placed at -120° and 120° , a tilting of the antennas can force the electromagnetic wave to reach the feeding point of the antennas at the same time. Therefore, by tilting the antennas by 30° the phase center will not be disturbed as

much as the previous case. Figure 6.27 shows the setup of the antennas.



Figure 6.27: Antenna setup offset at 30°.

The test setup was simulated in the same way as the previous test with the same credential. Results from the simulations of this setup can be seen in Figure 6.28.

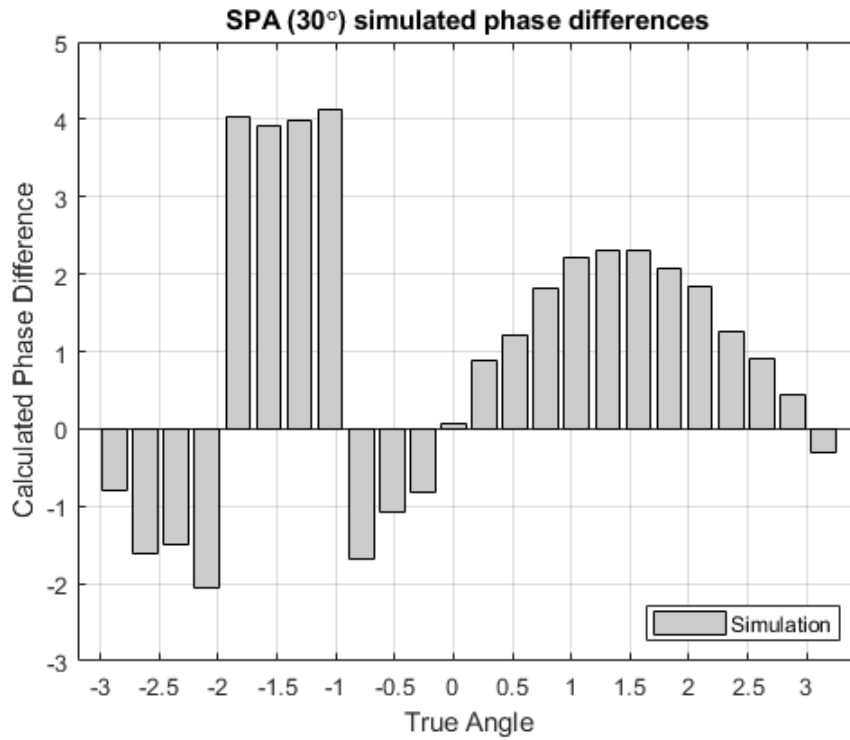


Figure 6.28: Simulated phase differences between the two standard patch antennas (30°).

After that the IQ samples were calculated using the equations 6.6, 6.2, 6.3 and 6.4. Using the IQ samples and the equation 6.5, the resulting phase differences can be seen in Figure 6.29.

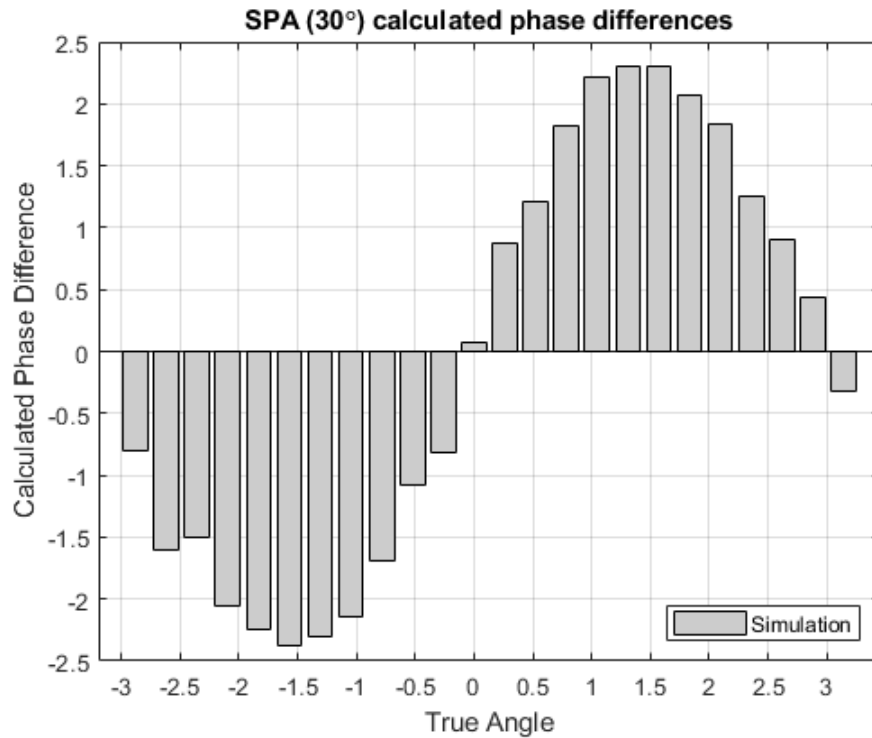


Figure 6.29: Calculated phase differences between the two standard patch antennas (30°).

The results show that the algorithm is compensating for the drifted angles when the antennas are tilted by 30° . In this case the speed is the same as the speed of the electromagnetic wave operating at channel 38 and the distance between the antennas is 52mm. The next step is to normalize the angles according to the wavelength operating and the distance between the receiver antennas. Figure 6.23 shows the results.

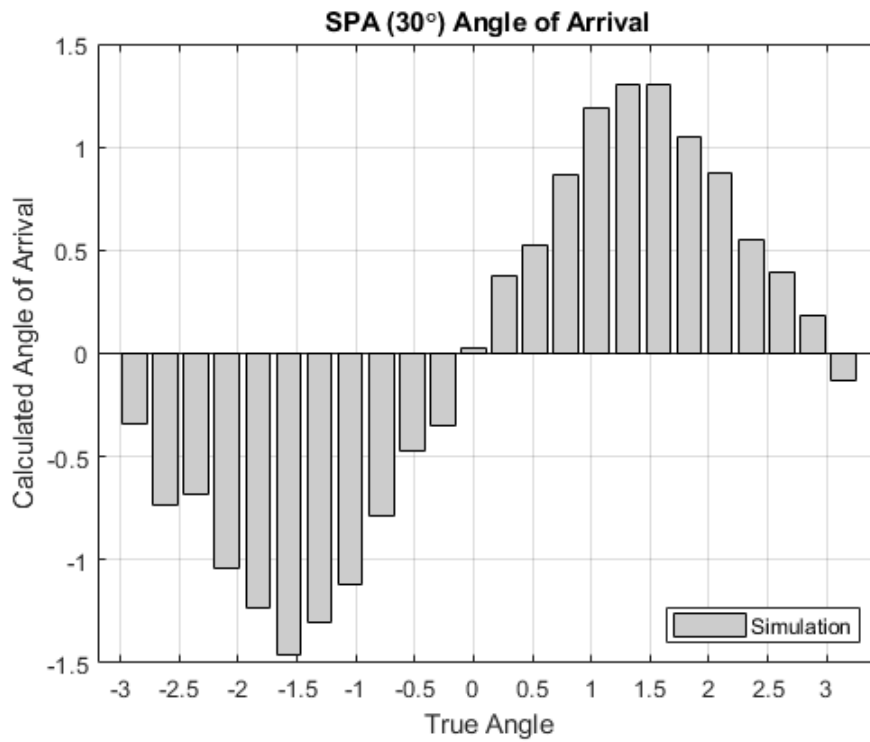


Figure 6.30: Calculated Angle of Arrival between the standard patch antennas (30°).

The results have improved drastically. However the accuracy decreased a lot.

The same test setup was used in an experiment in the EMC chamber. The credential was placed at a horizontal polarization at a distance of $0.7m$. The results can be seen in Figure 6.31.

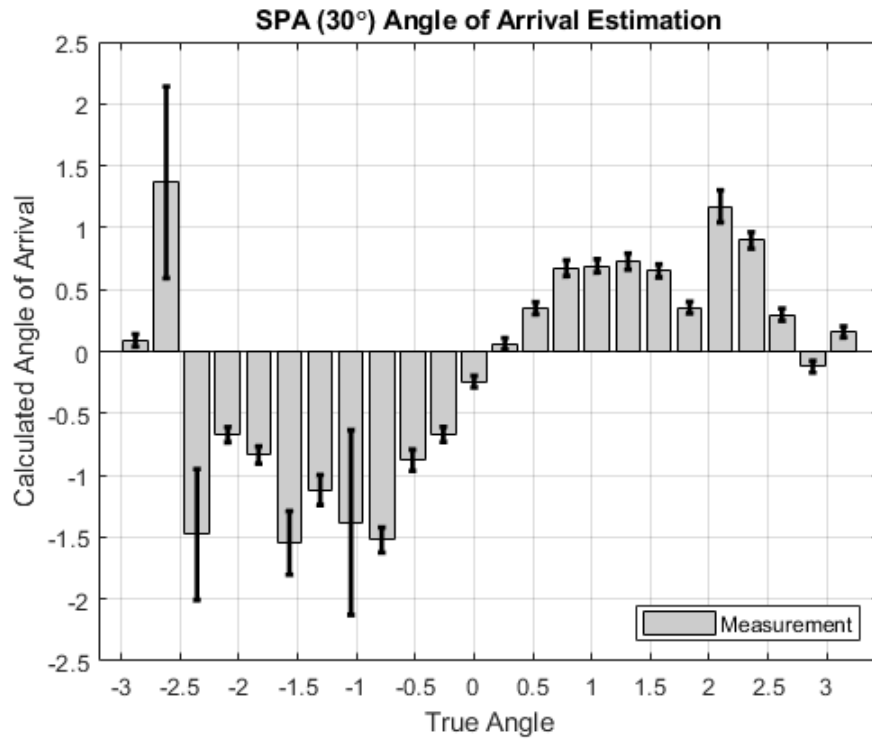


Figure 6.31: Angle of Arrival Estimation using the standard patch antennas (30°).

The results from this simulation are the best so far. There is a problem with the accuracy, but most of the angles have the correct sign. In addition, there are measured angles that have a relatively big variance. Figure 6.32 shows the results if the angles with a high variance are taken out.

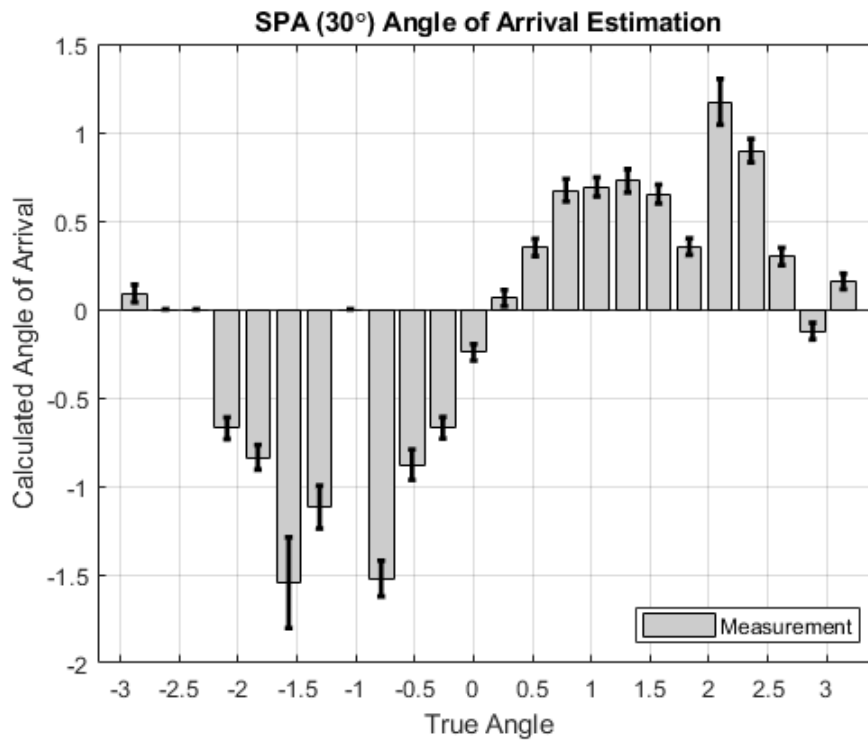


Figure 6.32: Angle of Arrival Estimation using the standard patch antennas (30°) after filtering.

After filtering out the angles with a high variance, the Figure is neater. The resulting angles are not satisfactory though.

Test Three

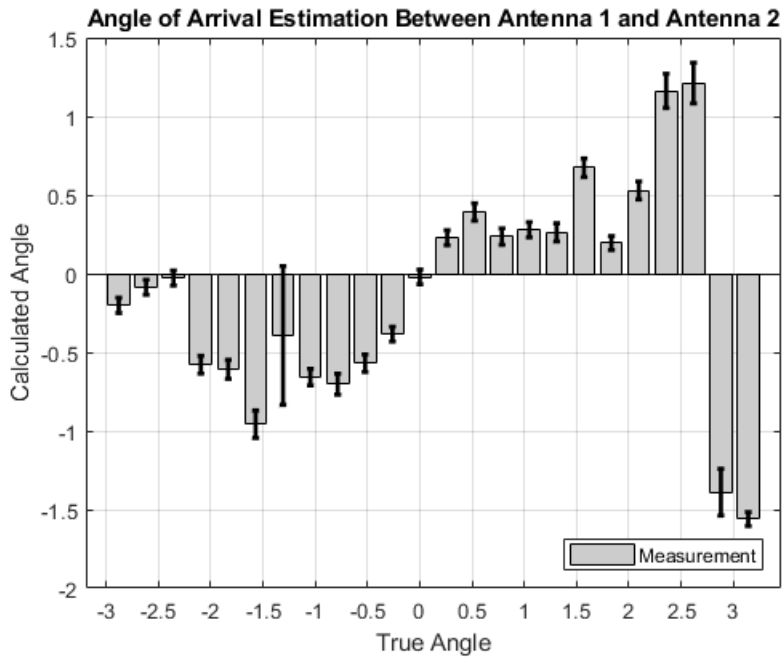
At this point in the project, it seems that a correct AoA estimation based on pure interferometry will be extremely difficult to achieve. However, since the antenna system is able to distinguish between left and right there is potential implementation in an inside-outside estimation based on angles. Therefore a third antenna will be added to the system behind the first antenna. This way the reference line will be perpendicular to the imaginary line passing through the two antennas. The angles that this system provides will give a potential solution in an inside-outside scenario.

Figure 6.33 depicts the antenna system.

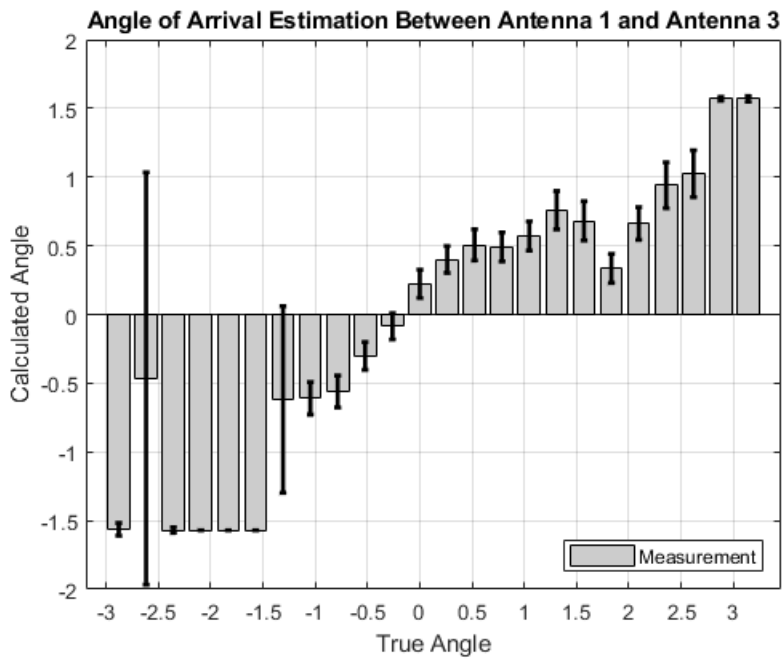


Figure 6.33: The three antenna system.

The resulting angles can be seen in Figure 6.34. Figure 6.34a shows the Angle of Arrival between antenna 1 and antenna 2. Figure 6.34b shows the Angle of Arrival between antenna 1 and antenna 3.



(a) Angle of Arrival estimation between A1 and A2.



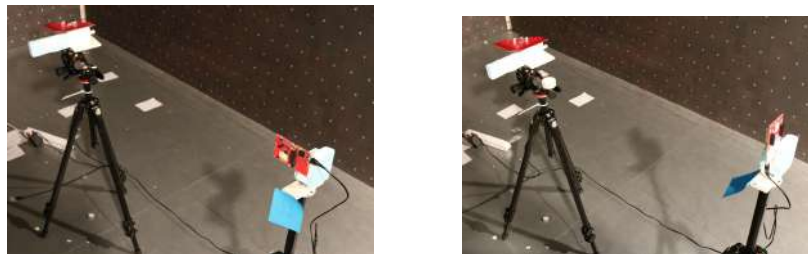
(b) Angle of Arrival estimation between A1 and A3.

Figure 6.34: The resulting angles from the three different antennas.

Figure 6.34b shows that an inside-outside solution could be achieved. The system decides if the credential is in front of the antenna system or behind depending on the sign of the resulting angle. Specifically, if the sign is positive then the credential is in front of the antenna system while when the sign is negative, the credential is behind the antenna system. The system has huge errors in the -60° and -150° regions. Unfortunately, the antenna design did not provide accurate results. The problematic angles could potentially accept a credential when the credential is on the opposite side. However rejecting the regions with a big amount of errors in the form of variance could solve the problem.

6.2.2 Credential Orientation

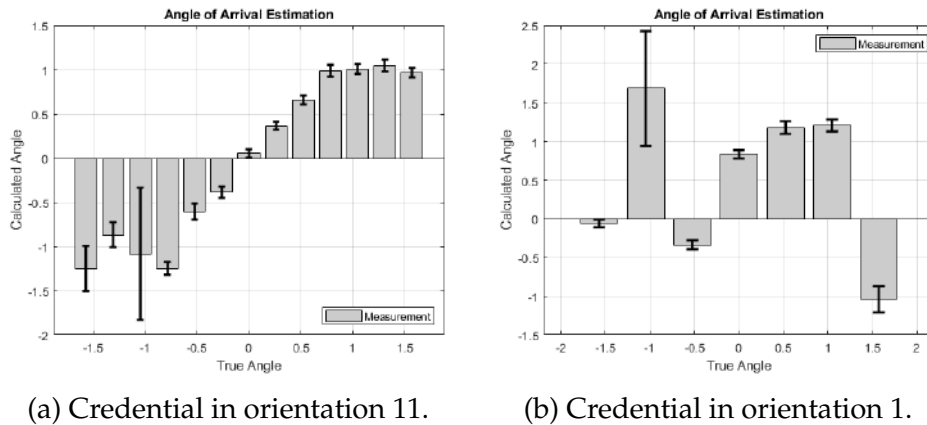
In this section the impact of the credential orientation will be presented. The credential has been put in two different orientations so that the vertical and horizontal linear orientation can be tested. The BSA antenna is linearly polarized and more specifically horizontally polarized in regards to the earth's horizon. In the following figures the measured angles when the credential is oriented to achieve different polarization in Figures 6.35a and 6.35b respectfully.



(a) Credential in orientation 11. (b) Credential in orientation 1.

Figure 6.35: Two different orientations of the credential.

The results from the two different credential orientations are presented in Figures 6.36a and 6.36b.



(a) Credential in orientation 11.

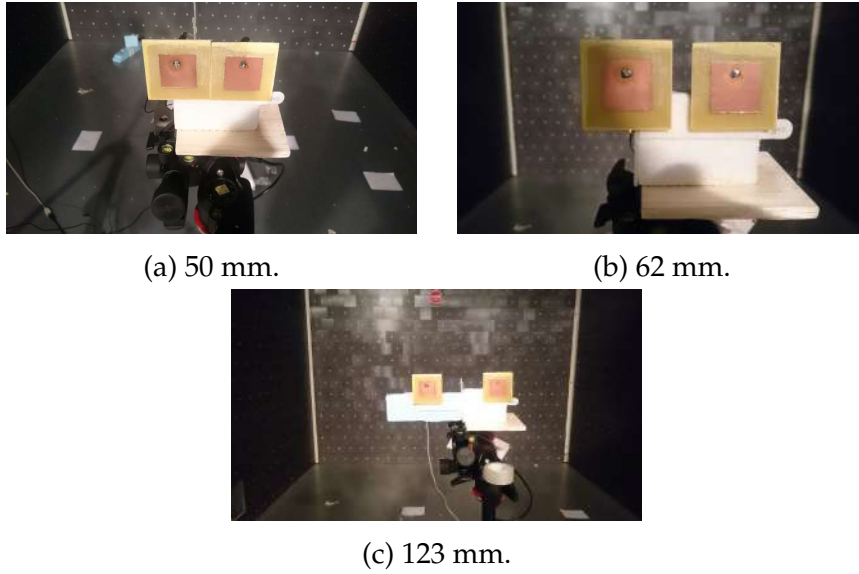
(b) Credential in orientation 1.

Figure 6.36: The resulting angles from the two different orientations of the credential.

It can be clearly seen how the credential orientation impacts the accuracy of the measurements. The antenna elements orientations in the system must be thoroughly considered before an implementation is made. A solution to this problem is an antenna system that uses circular polarization. However the design of circularly polarized antennas is much more complicated.

Distance Between Antennas

The distance between the antenna elements also plays a big role. There were three tests conducted where the antennas were placed at 50 mm, 62 mm and 123 mm apart. Figures 6.37a, 6.37b and 6.37c show how the antennas were separated.



(a) 50 mm.

(b) 62 mm.

(c) 123 mm.

Figure 6.37: The three different distances.

The results from the three different separations distances between the antenna elements are shown in Figure 6.38. Figures 6.38a, 6.38b and 6.38c show the measured angles for separation distances 50 mm, 62 mm and 123 mm.

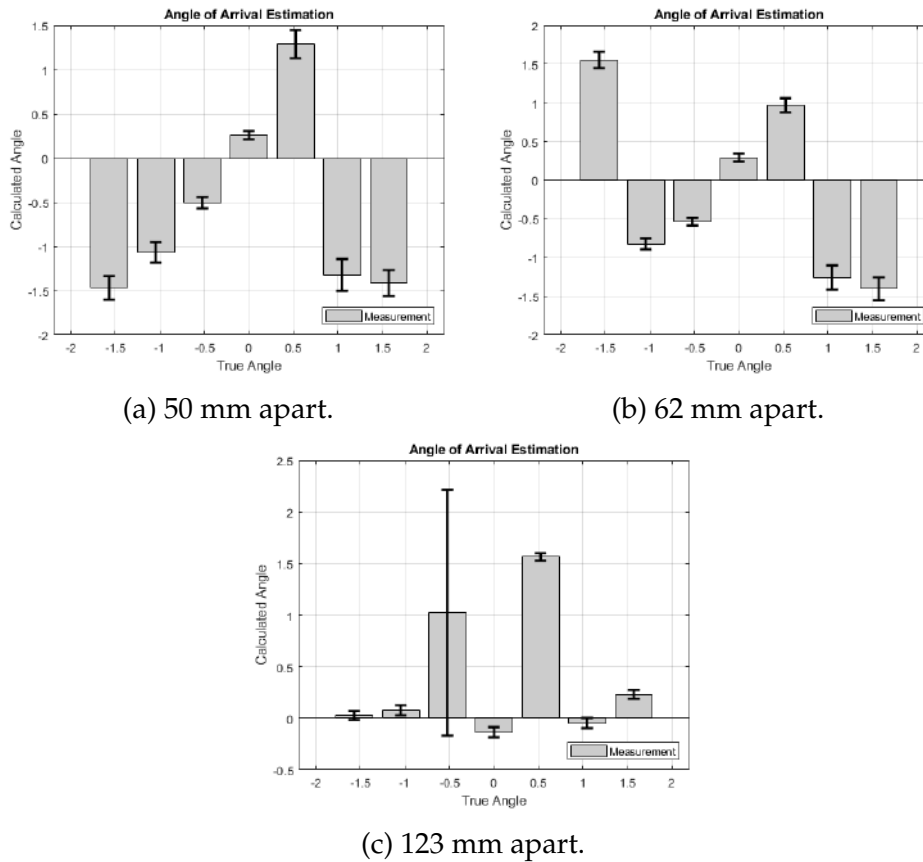


Figure 6.38: The resulting angles from the difference in the distance between the antenna elements.

BSA Summary

In the end it has been proved difficult increase accuracy. Especially, the angle at -60° shows consistently bad results in all tests. Filtering can help but it still cannot be solved entirely. In [21] has shown that between 60° and 120° and -60° and -120° the measurement errors are increased dramatically. Therefore reflection, coupling, noise and antenna related errors are increased to the point that filtering does not improve the result. The problem persists in both the EMC chamber and in the LoS lab.

Chapter 7

Conclusion

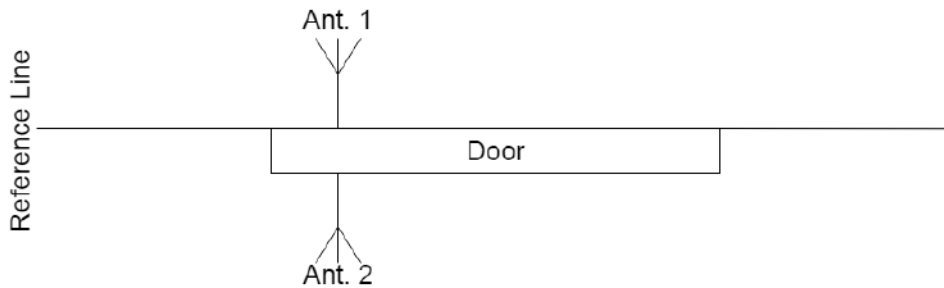
In this thesis, an analysis of the challenges the antenna designer faces when an AoA solution is desirable was made. A few antenna types have been designed, simulated, manufactured and tested on a prototype. The simulations were consistent with the theory, while the prototype held inconsistent results. The biggest problem in this project was to converge the simulation with the prototype results. The antenna type SPA did manage to converge the results. The differences can be attributed to the fact that there was hardware, cables and other testing equipment nearby which interfered with the results. In addition it has been tested that the switching board is unbalanced.

It is apparent from the simulations that the credential's different orientations exhibit similar results. However, the measurements show that the credential orientation can drastically change the results. This is consistent with similar studies that have tested different credential orientations.

However, the results show that a possible implementation can be indeed made. In the case of an inside-outside scenario, the system has to distinguish if the credential is inside or outside of a reference line. This means that this is a binary choice. Two antennas that are placed in such a way that they create a reference line that concurs with the line that outlines between inside and outside. Therefore, a system implementing AoA can use two antennas in this configuration to calculate the sign of the measured angle. The sign can be either positive or negative which shows between inside and outside. Figure 7.1 makes it more clear. An angle that has a plus sign shows that the credential is outside and therefore the door will open. On the other hand, an angle

that has a negative sign shows that the credential is inside and therefore the door will not open. This can simplify the system since the accuracy of the sign of the measured angle is important in this case.

Outside/-



Inside/+

Figure 7.1: A potential use of AoA in access control applications.

7.1 Future studies

There is a great number of future studies that could be conducted. As it can be seen from the studies provided in the references, the authors have identified potential problems and recommended solutions. Proposed studies include testing antennas that have similar minimum gain or higher as the SPA and a size smaller in order to reduce the phase center implications.

In addition, a new model for a similar system should be investigated. This model should be more specific to the system and take into consideration the attenuation losses of all the hardware involved.

Finally, readers are encouraged to investigate further the limitations of the phase interferometry solutions with the absence of adaptive algorithms in order to specify guidelines for engineers designing antennas for AoA.

References

- [1] Statista, “Number of smartphone users worldwide from 2014 to 2020 (in billions)”, 2018.
- [2] Statista, “Projected size of the global market for RFID tags from 2016 to 2020 (in billion U.S. dollars)”, 2018.
- [3] M. Hughes, “The Incredible Shrinking Circuit: Small PCBs and Smaller ICs in 2018”, <https://www.allaboutcircuits.com/news/the-incredible-shrinking-circuit/>, Last accessed on 2018-09-25.
- [4] Balanis, “Antenna Theory Analysis and Design”, vol. Third Edition, 2005.
- [5] S. O. Al-Jazzar, H. J. Strangeways, and D. C. McLernon, “2-D Angle of Arrival Estimation Using a One-Dimensional Antenna Array”, *2014 22nd European Signal Processing Conference (EU-SIPCO)*, 1-5 Sept. 2014.
- [6] R. Schmidt, “Multiple emitter location and signal parameter estimation”, *IEEE Transactions on Antennas and Propagation*, 1986.
- [7] S. Wielandt, J.-P. Goemaere, and L. D. Strycker, “Multipath-Assisted Angle of Arrival Indoor Positioning System in the 2.4 GHz and 5 GHz Band”, *2016 International Conference on Indoor Positioning and Indoor Navigation (IPIN)*, 2016.
- [8] IEEE, “IEEE Standard for Information technology – Telecommunications and information exchange between systems Local and metropolitan area networks–Specific requirements - Part 11: Wireless LAN Medium Access Control (MAC) and Physical Layer (PHY) Specifications”, 2016.

- [9] B. Sahinbas, L. Weisgerber, and M. Schuhler, "AoA and Source Polarization Estimation with Circularly Polarized Multibeam Antenna using MUSIC Algorithm", *11th European Conference on Antennas and Propagation (EUCAP)*, 2017.
- [10] A. Lavrenko, S. Pawar, M. Ibrahim, F. Romer, G. D. Galdo, and R. S Thomä, "Combining Matrix Design for 2D DoA Estimation with Compressive Antenna Arrays", *WSA 2018*, 2018.
- [11] T. A. de B. Gripp, B. M. Fabiani, E. S. Silveira, and D. C. Nascimento, "Design of a Microstrip Antenna Array with Polarization Diversity for DoA Application with Compressive Antenna Arrays", *2017 SBMO/IEEE MTT-S International Microwave and Optoelectronics Conference (IMOC)*, 2017.
- [12] Y. Xie, C. Peng, X. Jiang, and S. Ouyango, "Hardware Design and Implementation of DOA Estimation Algorithms for Spherical Array Antennas", *2014 IEEE International Conference on Signal Processing, Communications and Computing (ICSPCC)*, 2014.
- [13] S.-C. Cheng and K.-C. Lee, "REDUCING THE ARRAY SIZE FOR DOA ESTIMATION BY AN ANTENNA MODE SWITCH TECHNIQUE", *Progress In Electromagnetics Research*, vol. 131, no. 117–134, 2012.
- [14] IEEE, "IEEE Standard Definitions of Terms for Antennas", 1973.
- [15] L. Learning, "Electromagnetic Waves and their Properties", [Online]. Available: <https://courses.lumenlearning.com/boundless-physics/chapter/electromagnetic-waves-and-their-properties/> (visited on 07/12/2018).
- [16] M. S. Neiman, "The Principle of Reciprocity in Antenna Theory", *Proceedings of the IRE*, vol. 31, no. 12, 1943.
- [17] P. J. Bevelacqua, "The Antenna Theory Website", 2009.
- [18] I. E. Commission, "Antennas", 712-02-42,
- [19] IEEE, "IEEE Standard Definitions of Terms for Antennas", *IEEE Standards*, vol. 145-1973, 1973.
- [20] B. SIG, "BLUETOOTH CORE SPECIFICATION Version 5.1 | Vol 0, Part A", 21 January 2019.
- [21] M. Englund, "Evaluation of Angle of Arrival based positioning for keyless entry access control", 2018.

- [22] S. Choudhury, "Effect of Dielectric Permittivity and Height on a Microstrip-Fed Rectangular Patch Antenna", *IJECT*, vol. 5, no. 2, 2014.
- [23] A. Khan and R. Nema, "Analysis of Five Different Dielectric Substrates on Microstrip Patch Antenna", *International Journal of Computer Applications*, vol. 55, no. 18, 2012.
- [24] T. Instruments, "CC2640R2F SimpleLink™ Bluetooth® low energy Wireless MCU", January 2017.
- [25] T. Instruments, "2.4-GHz Inverted F Antenna", 2017.
- [26] Digi, "Indoor Path Loss", 2012.
- [27] I. T. Union, "PROPAGATION DATA AND PREDICTION MODELS FOR THE PLANNING OF INDOOR RADIOCOMMUNICATION SYSTEMS AND RADIO LOCAL AREA NETWORKS IN THE FREQUENCY RANGE 900 MHz TO 100 GHz", *International Telecommunications Union*, vol. RECOMMENDATION ITU-R P.1238, 1997.
- [28] S. Wielandt, M. V. Shah, N. A. Athaullah, U. M. Sayyad, R. B. Yadav, R. M. Dharamdasani, L. D. Strycker, and M. Kuhn, "2.4 GHz Single Anchor Node Indoor Localization System with Angle of Arrival Fingerprinting", 2017.
- [29] K. Cafe, "Electronic Warfare and Radar Systems Engineering Handbook - Polarization -", <http://www.rfcafe.com/references/electrical/ew-radar-handbook/polarization.htm>, Last accessed on 2018-07-10.
- [30] S. L. Enrique G. Plaza German Leon and L. F. Herran, "Calculating the Phase Center of an Antenna: A Simple Experimental Method Based on Linear Near-Field Measurements. [Measurements Corner]", October 2017.
- [31] T. Instruments, "SimpleLink™ Angle of Arrival BoosterPack", <http://www.ti.com/tool/BOOSTXL-AOA>, Last accessed on 2018-12-19.
- [32] J.-W. Yang, T.-Y. Tsai, C.-C. Chan, and C.-Y.-D. Sim, "Small size circularly polarized patch antenna for 2.4 GHz WLAN applications", *2016 IEEE 5th Asia-Pacific Conference on Antennas and Propagation (APCAP)*, pp. 153–154, 2016.

- [33] T. America, "LIQUID PHOTOIMAGEABLE SOLDER MASK - PSR-4000 CC01SE DI -", 2016.
- [34] S. Ghosal and S. R. B. Chaudhuri, "Analysis of a rectangular slot on a microstrip patch antenna with an equivalent circuit model", *2013 IEEE Applied Electromagnetics Conference (AEMC)*, 2013.
- [35] W. Junjun, "Compact circularly polarized MSA ", *School of Electronic and Information Engineering, Beihang University*,
- [36] T. Instruments, "CC2640R2F SimpleLink™ Bluetooth® low energy Wireless MCU datasheet (Rev. A)", 2017.
- [37] H. Booker, "Slot aeriels", *Journal of the Institution of Electrical Engineers - Part IIIA: Radiolocation*, vol. 93, 1946.

